"A SENSITIVE TURN OFF – TURN ON FLUORESCENT PROBE FOR DETECTION OF BIOTHIOLS USING MnO_2@CARBON DOTS"

A
Thesis submitted
Inpartial fulfilment of the requirements for the degree of

MASTERS OF SCIENCE
IN
CHEMISTRY

Submitted by

DIMPLE GARG
(301502013)
Under the Supervision of

Dr.SOUMEN BASU
(Associate Professor)

SCHOOL OF CHEMISTRY & BIOCHEMISTRY

THAPAR UNIVERSITY, PATIALA

July, 2017

CERTIFICATE

I hereby declare that the thesis entitled **"A Sensitive Turn Off – Turn On Fluorescent Probe for Detection of Biothiols Using MnO_2@Carbon Dots"** is an authentic record of my work carried out as requirements for the award of the degree of Master of Science in Chemistry at Thapar University, Patiala under the supervision of Dr. Soumen Basu, Associate Professor, School of Chemistry & Biochemistry, Thapar University, Patiala during July' 2015 to July' 2017. No part of the matter embodied in this report has been submitted to any other university or institute for the award of any degree.

Dimple

Dimple Garg

Date: 14/07/2017

It is certified that the above statement made by the student is correct to the best of my knowledge and belief.

S. Basu

Dr. Soumen Basu
Associate Professor
School of Chemistry & Biochemistry
Thapar University, Patiala - 147004

CANDIDATE'S DECLARATION

I hereby declare that the work being presented in the dissertation entitled **"A Sensitive Turn Off – Turn On Fluorescent Probe for Detection of Biothiols Using MnO_2@Carbon Dots"** in partial fulfilment of the requirements for the award of degree of Masters of Science in Chemistry and being submitted to School of Chemistry and Biochemistry, Thapar University, Patiala, is my own work during the period of January' 2017 to July' 2017, under the supervision of **Dr. Soumen Basu.** I have not submitted the contents embodied in this dissertation for the award of any other degree.

Patiala
Date: 14/07/2017

Dimple

Dimple Garg

This is to certify that the statement made by the candidate is correct and true to the best of our knowledge.

S Basu P.

Dr. Soumen Basu
Associate Professor
School of Chemistry & Biochemistry
Thapar University, Patiala – 147004

ACKNOWLEDGEMENT

First of all, I would take up this opportunity to thank my Supervisor, Dr.SoumenBasufor his guidance and constant motivation to work hard for the successful completion of my project.

I own a deep sense of gratitude towards Dr.Amjad Ali (Associate Professor and Head, School of Chemistry & Biochemistry) and all the faculty members for their timely support and help.

I would also like to thank**Ms. Akansha Mehta**, **Mr. Amit Mishra**, **Ms. ShagunKainth**, **Ms. Manisha Sharma**, **Ms. ShrutiParashar** and **Ms. Nidhi Arora**who never turned me down whenever I approached them for any kind of help. Not to forget, I am grateful to all other research scholars also for their assistance.

I am thankful to **School of Chemistry & Biochemistry, Thapar University** for providing me the opportunity to carry out this 6-months research experience and also, for the availability of facilities that were required for the successful completion of my work.

Words are just not enough to express my gratitude towards my family and friends who have always supported me and have been a source of strength and inspiration to me during the entire period of the work.

All these thanks are, however, only fraction of what is due to almighty for granting me an ever-willingness and strength to successfully accomplish this project.

ABSTRACT

Presently, the combination of carbon quantum dots (CQDs) and metal oxide nanostructures in one frame are being considered for the sensing of purine compounds. In this work, a combined system of CQDs and MnO_2 nanostructures was used for the detection of anticancer drugs – 6-Thioguanine (6-TG) and 6-Mercaptopurine (6-MP). The CQDs were synthesized using bottom-up approach through microwave synthesizer and the MnO_2 nanostructures (nanoflowers and nanosheets) were synthesized using facile hydrothermal technique. The CQDs exhibited excellent fluorescence emission at 420 nm when excited at 320 nm wavelength. When combining CQDs and MnO_2 nanostructures, quenching of fluorescence was observed which was attributed to fluorescence resonance energy transfer (FRET) mechanism, where CQDs act as electron donor and MnO_2 nanostructures act as acceptor. This fluorescence quenching behaviour disappeared on the addition of 6-TG and 6-MP due to the formation of Mn-S bond. The detection limit (LOD) of 0.01 μM for 6-TG and 6-MP was achieved with the linear range of concentration of 0-50 μM using both MnO_2nanoflowers (NF) and nanosheets (NS). Moreover, the as-prepared fluorescence-sensing technique was successfully employed for the detection of bio-thiol group in enapril drug. Thus a facile, costeffective and benign chemistry approach for biomolecule detection was designed.

Key words:

Carbon quantum dots, MnO_2, nanoflowers, nanosheets, 6-Thioguanine, 6-Mercaptopurine, fluorescence turn off – turn on.

CONTENTS

LIST OF FIGURES

LIST OF TABLES

LIST OF ABBREVIATIONS AND SYMBOLS

1.	**TCPO**	bis(2,4,6-trichlorophenyl)oxalate
2.	**BET**	Brunauer-Emmett-Teller
3.	**CQDs**	Carbon quantum dots
4.	**CL**	Chemiluminescence
5.	**CRET**	Chemiluminescence Resonance Energy Transfer
6.	**Da**	Dalton
7.	**^{o}C**	Degree Celsius
8.	**DNA**	Deoxyribo-nucleic acid
9.	**dsDNA**	Double-stranded deoxyribo-nucleic acid
10.	**DLS**	Dynamic light scattering
11.	**λ_{em}**	Emission wavelength
12.	**EDX/EDS**	Energy dispersive X-ray spectroscopy
13.	**FL**	Fluorescence
14.	**FRET**	Förster Resonance Energy Transfer
15.	**AuNPs**	Gold nanoparticles
16.	**>**	Greater than
17.	**H**	Hours
18.	**<**	Less than
19.	**LSPR**	Localized surface plasmon resonance
20.	**λ_{max}**	Maximum wavelength
21.	**MΩ**	Mega ohm
22.	**MP**	6-Mercaptopurine
23.	**M**	Metre
24.	**µL**	Micro litre
25.	**µM**	Micro molar
26.	**Ml**	Millilitre
27.	**MW**	Molecular Weight
28.	**NF**	Nanoflowers

29.	**Nm**	Nanometre
30.	**NPs**	Nanoparticles
31.	**NS**	Nanosheets
32.	**%**	Percent
33.	**PL**	Photoluminescence
34.	**QDs**	Quantum dots
35.	**SEM**	Scanning electron microscope
36.	**AgNPs**	Silver nanoparticles
37.	**SERS**	Surface-enhanced raman spectroscopy
38.	**TG**	Thioguanine
39.	**TEM**	Transmission electron microscope
40.	**UV-Vis**	Ultraviolet-Visible
41.	**W**	Watt
42.	**XRD**	X-ray diffractometer
43.	**XPS**	X-ray photoelectron spectroscopy

CHAPTER 1

INTRODUCTION

1.1 Nanoparticles

1.1.1 Overview

Nano, like milli, micro, pico, and so on, is a prefix used in front of a macroscopic unit to change its value by orders of magnitude. Nano means one billionth, or 10^{-9}. Thus, one nanometre is one billionth of a metre [1]. Figure 1.1 given below illustrates the scale to represent different dimensions.

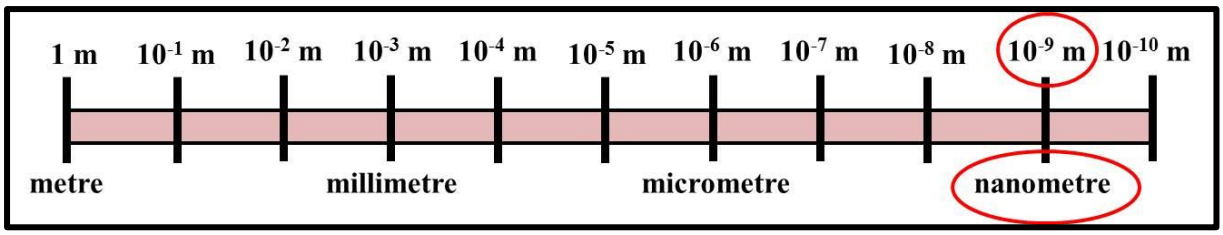

Figure 1.1 A Scale to Represent Different Dimensions.

In science and technology, it implies studying and employing matter with the smallest dimensions ranging from a few nanometres to less than 100 nanometres. These materials which have sizes in the range of 1-100 nm are known as nanoparticles. Nanoscience and nanotechnologies comprise a range of techniques and stretch across the whole variety of science fields, touching medicine, physics, engineering and chemistry. They are widely known to be highly beneficial in areas as diverse as drug development,water decontamination, information and communication technologies, and the production of stronger, lighter materials. In chemistry, this range of sizes has generally been associated with colloids, micelles, polymer molecules, phase-separated regions in block copolymers, and similar structures—typically, very large molecules, or aggregates of many molecules [2]. Due to the intermediate sizes of nanoparticles in between those of individual atoms (and molecules) and those of bulk solids, they fail to obey both of the absolute quantum chemistry and the laws of classical physics. The size of the particle reduces leading to increase in surface-to-volume ratio. Also, the properties of a nanoparticle are sensitive to the size of these particles. The effect specific to the small size of nanoparticles is called the quantum size effect (QSE) [3] which allows to synthesize particles and designs with a variety of properties.

1.1.2 Synthesis Strategies

There are two general approaches to the synthesis of nanomaterials and the fabrication of nanostructures: “Top-down” and “Bottom-up” approaches. As the names suggest, the top-down approach implies going from larger to smaller and the bottom-up approach involves going from smaller to larger. In top-down approach, bulk-material (macroscopic) is fragmented into fine particles progressively and in bottom-up approach, atoms and molecules are combined together to synthesize nanoparticles. The bottom-up approach yields nanomaterials with lesser imperfections, homogenous chemical-composition, fewer impurities, and materials with a fine size-distribution. The top-down method typically leads to the formation of smaller fragments or materials with an extensive size-distribution which is actually the main drawback of this approach. Therefore, the bottom-up method is significantly modest and specific for preparation of nanomaterials with size < 100 nm, and the top-down method is favoured for the preparation of thin-films and nanomaterials > 100 nm [4]. A schematic representation of the “Top-down” and “Bottom-up” methods is shown in Figure 1.2.

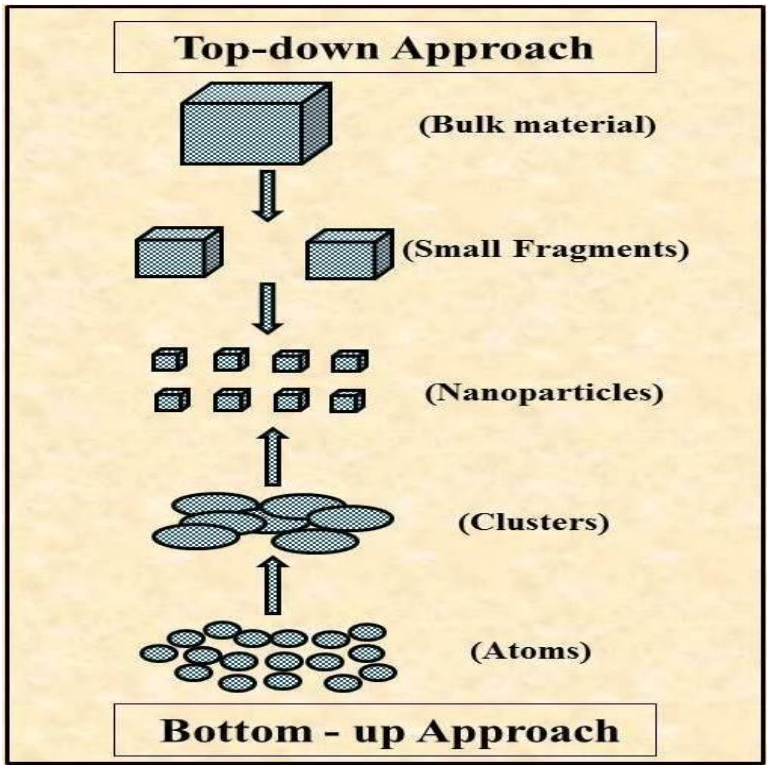

Figure 1.2Schematic Representation of "Top-down" and "Bottom-up" Approaches.

1.2 Carbon Quantum Dots (CQDs)

1.2.1 Overview

Quantum Dots (or QDs) are actually the semiconductor nanocrystals. They are prepared from atoms of groups II-VI or III-V in the periodic Table. The quantum dots have comparatively smaller exciton Bohr radius (EBR) than the bulk material. In the last few years, developments have been made in the nanoparticles for applications in the fields of biology and medicine. The significant research in the production of fluorescent quantum dots with high yields, complex surface-chemistry, water-solubility, bio-compatibility and eco-friendliness has helped greatly in the sensitive sensing of bio-molecules. Latest progresses have presented quantum dots for intracellular-imaging, nano-drugs for various specific therapies, syndrome monitoring, sensing and analysis. Interestingly, these were actually discovered accidently in 2004 by Xu et. al when this group was purifying single-walled carbon nanotubes. These carbon quantum dots then triggered much concern as potential competitors to conventional semiconductor quantum dots [5]. In addition to their comparable optical properties, CQDs have the desired advantages of low toxicity, inexpensive and relatively simpler routes of synthesis [6]. The chemical structure of CQDs is shown in Figure 1.3 and the fluorescence spectrum of CQDs has been illustrated in Figure 1.4.

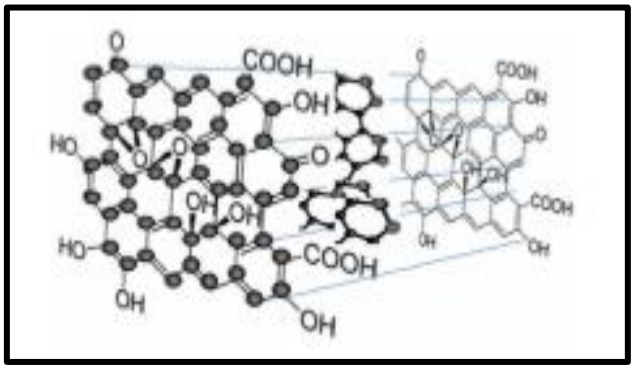

Figure 1.3 Chemical Structure of CQDs [7].

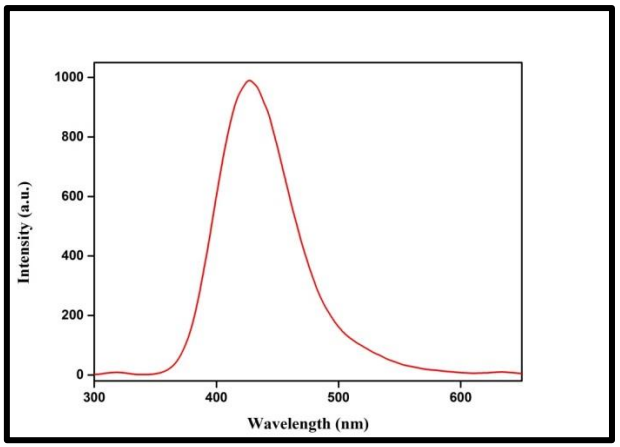

Figure 1.4 Fluorescence Spectra of CQDs.

1.2.2 Applications of Carbon Quantum Dots

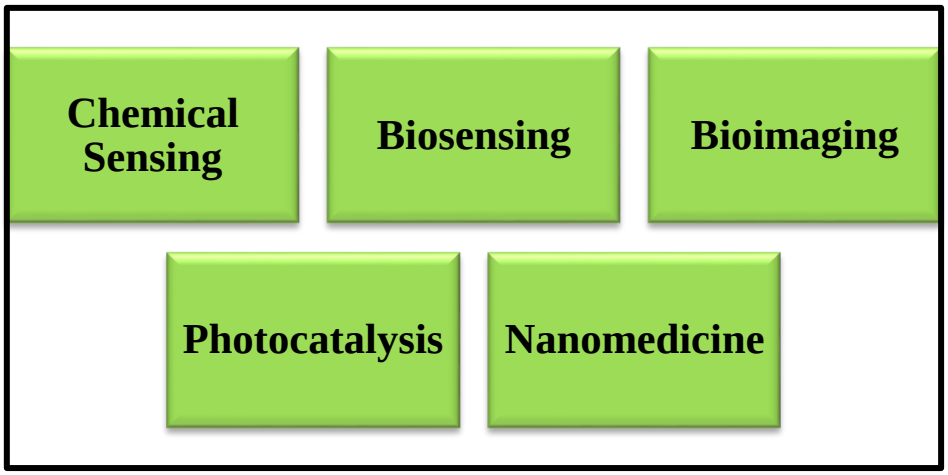

Figure 1.5 Applications of CQDs.

Chemical Sensing

CQDs have been used extensively to detect various chemical compounds as well as metal ions such as DNA, phosphate, thrombin, nitrite, glucose, Iron(III), Hg_2^{2+}, etc. by analysing the change is fluorescence intensity under external physical or chemical conditions [8].

Biosensing

CQDs being highly soluble in water, flexible in surface modification, benign, biocompatible, cell permeable and highly stable along with the fascinating property of exhibiting excitation-dependent multicolour emission, have been exploited greatly as biosensors for the detection of glucose, cellular copper, PO_4^{3-}, Fe^{3+}, nucleic acids, etc[8].

Bioimaging

CQDs have numerous benefits such as excellent optical properties and photostability. Also, carbon is benign and eco-friendly. These qualities make them significant substitutes to conventional semiconductor quantum-dots to monitor biological systems both in vitro and in vivo [7].

Photocatalysis

Over the past few years, photocatalysis has attracted significant attention as greener substitutes in organic synthesis. Because of sunlight being an efficient and unlimited energy resource, huge concern towards the photocatalyst processes has been observed. But, the organic compounds and moieties are affected poorly due to high energy of UV and short

wavelength of Visible light. The ability to undergo exchange of energy with the CQDs and availability of light of longer wavelength offers a tremendous prospect for these to be used in the photocatalysis[7].

Nanomedicine

CQDs are considered in nanomedicine because they are absolutely benign for animals and therefore are well exploited for carrying out the studies in-vivo. This has been demonstrated by in-vivo toxicity studies in mice, whereby the mice were injected with CQDs and observed after a month. None of the organs and internal functions got damaged or affected in any way [7].

1.3 MnO_2 Nanostructures

1.3.1 Overview

The arrangement of fluorescent materials and other functional nanomaterials in one matrix have been broadly employed in the assembly of efficient sensors. Nanomaterials, such as gold nanoparticles, silver nanoparticles, graphene oxide [9, 10], molybdenum sulphide [10], gold nanoparticles [11], and silver nanoparticles [12] are good fluorescence-quenchers and have already been employed to improve fluorescent sensors for sensitive recognition of various analytes[12-14]. Manganese dioxide (MnO_2) NS and NF have high specific surface area and relatively better light-absorption and fluorescence-quenching capabilities. They have attracted considerable concern in emerging "turn off – turn on" fluorescence-sensing detectors [15, 16]. In present work, CQD-MnO_2 system has been used as a newly designed analytical tool for the efficient, selective and relatively faster detection of 6-TG and 6-MP. CQDs derived from ascorbic acid are very inexpensive and eco-friendly probe.

1.3.2 Different Shapes of MnO_2 Nanostructures

Till date, several developments have been made to synthesize MnO_2 nanostructures having different morphologies. The fluorescence quenching behavior of MnO_2 has been expected to be strongly influenced by a variety of factors including the morphologies of these nanostructures such as nanoflowers, nanosheets and nanospheres. The number of active sites and surface area of non-spherical nanostructures is known to be higher than those of spherical nanostructures.

1.4 Förster Resonance Energy Transfer (FRET)

FRETis a distance-dependent interaction between the electronic excited states of two molecules wherein overlapping between the emission spectrum of a donor molecule and the absorption spectrum of an acceptor molecule takes place. This phenomenon is also known as Fluorescence Resonance Energy Transfer. The acceptor may not be fluorescent. There is no involvement of emission of light (and photon) during resonance energy transfer. The extent of energy transfer is dependent on the distance between the donor and acceptor, and the extent of spectral overlap. The spectral overlap (Figure 1.6) is described in terms of the Förster distance (R_0). The rate of energy transfer $k_T(r)$ is given by:

$$k_T(r) = \frac{1}{\tau_D}\left(\frac{R_0}{r}\right)^6$$

where 'r' is the distance between the donor and acceptor and 'τ_D' is the lifetime of the donor in the absence of energy transfer.

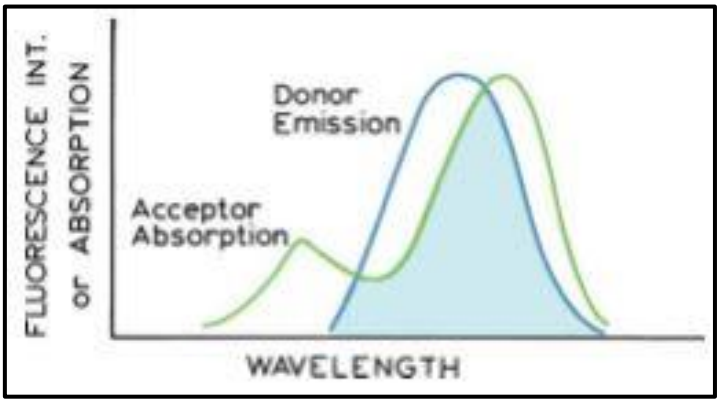

Figure 1.6 Spectral Overlap for Fluorescence Resonance Energy Transfer [18].

The efficiency of the FRET process depends on the inverse sixth power of the distance between the donor and acceptor pair (r) and is given by [17]:

$$\mathsf{E} = \frac{{R_0}^6}{{R_0}^6 + r^6}$$

1.5 Thioguanine&Mercaptopurine

Purine compounds play significant roles in human cell metabolism and are used in several cancer–treating medicines. 6-Thioguanine (6-TG) and Mercaptopurine (6-MP) are purine compounds used for the treatment of cancer such as acute lymphoblastic leukemia[19]. However, the concern of their dose is of critical significance, that is, the under-dosage will be unsuccessful in the cure of disease and quite adverse effects like bone marrow suppression and liver problems may be caused by their over-dosage [20]. Therefore, biosensors for 6-TG

and 6-MP detection have attracted considerable attention over the last few years. Recently, numerous techniques have been developed for the detection of these purine compounds such as fluorescence [20, 21], high performance liquid chromatography [22-26], electrochemical methods [27-29], surface-plasmon resonance [30].Most of these techniques have disadvantages of being tedious, labor-intensive, sophisticated instrumentation, or costly reagents, which limit their practical applications [31].

Hence, fluorescence sensors have been developed for the detection of these purine compounds and are being considered significantly, now-a-days.

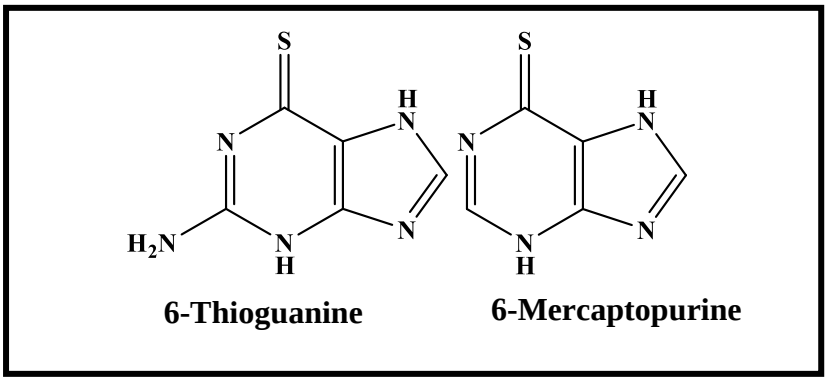

1.6 Fluorescence Turn Off – Turn On of Carbon Quantum Dots

The CQDs exhibit high fluorescence intensity as discussed before. However, with increasing concentration of MnO_2 nanostructures, the PL intensity of these CQDs decreases gradually. This phenomenon of quenching of fluorescence of CQDs by MnO_2 nanostructures is termed as Fluorescence turn-off. Interestingly, on addition of 6-TG (and 6-MP), the PL intensity shows an increase and it keeps on increasing with increasing concentration of these biomolecules. The process of restoration of fluorescence of CQDs by biomolecules is known as Fluorescence turn-on. The fluorescence turn off – turn on phenomena has been illustrated through the simple diagram in Figure 1.7.

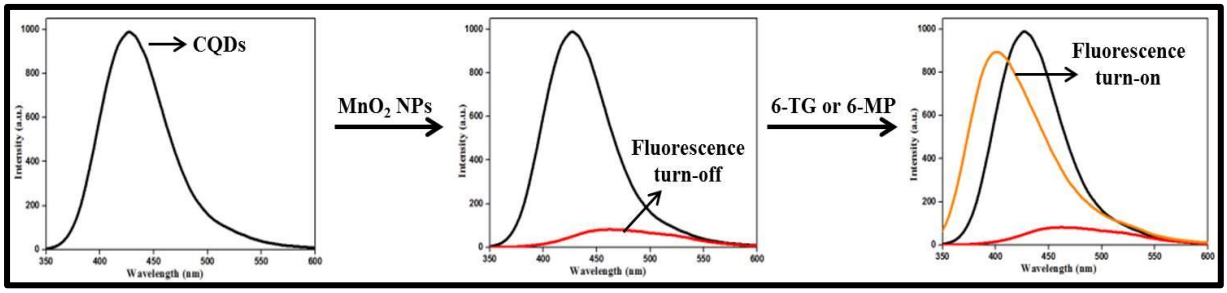

Figure 1.7 Fluorescence Turn Off - Turn On of CQDs.

CHAPTER 2

LITERATURE REVIEW

As discussed before, the detection of 6-TG and 6-MP has attracted a lot of attention in the past few years and are being used as anti-cancer drugs. The estimation of the quantities of both of these drugs during the course of injection into the body is very crucial. Therefore, numerous detection techniques have been designed till date. Some of these methods and designs have been discussed below in Table 2.1.

Table 2.1 Some of the techniques and designs developed till date.

S.No.	Group (Year)	Detection; Technique	Description	Reference
1.	Shen *et al.* (2005)	6-MP; Fluorescence	Fluorescent AuNPs assembled with 6-MP themselves and thus their fluorescent intensity increased remarkably due to aggregation of these NPs.	[32]
2.	Wang *et al.* (2006)	6-TG; Surface Electrochemical technique based on dsDNA film modified electrode.	They had fabricated a film consisting of dsDNA over 2-aminoethanethiol self-assembled monolayers film modified gold electrode by electrostatic adsorption and utilized $[Fe(CN)_6]^{3-/4-}$ and $[Co(bpy)_3]^{2+/3+}$ to examine the contact between dsDNA and 6-TG.	[26]
3.	Zhang *et al.* (2008)	6-MP; Molecular Imprinted Polymer (Fluorescence)	This optical fibre sensor modified 6-MP by carrying out its oxidation to form a compound which exhibited fluorescence.	[33]
4.	Chen *et al.* (2012)	6-MP; Fluorescence	Fluorescent AuNPs were stabilized by biomacromolecules. With variable concentration of 6-MP, variety of colors were observed under the UV-lamp.	[34]

5.	Du *et al.* (2012)	6-MP; CRET	Chemiluminescent bis(2,4,6-trichlorophenyl) oxalate (TCPO) – H_2O_2 – fluorescein acted as donor and AuNPs acted as acceptor. CRET resulted in quenching of CL of the TCPO – H_2O_2 – fluorescein reaction which was again restored in the presence of 6-MP. The restoration of CL was complemented by a change in color and optical properties.	[35]
6.	Bi e*t al.* (2013)	6-TG; LSPR	Interaction between 6-TG and AuNPs led to the shift in the LSPR spectrum.	[28]
7.	Amjadi*et al.* (2014)	6-TG; Fluorescence	Fluorescent harmine acted as donor and AgNPs acted as acceptor. FRET resulted in quenching of fluorescence. However, on addition of 6-TG, the fluorescence got restored due to the adsorption of these bio-molecules over AgNPs.	[21]
8.	Maleh*et al.* (2015)	6-MP; Differential Pulse Voltammetry	Utilized DNA over a pencil graphite electrode which was modified with polypyrrole and functionalized multiwalled carbon nanotubes. Differential Pulse Voltammetry was used to detect the interaction of 6-MP and dsDNA.	[36]
9.	Tian *et al.* (2016)	6-TG; SERS	AgNPs – coated silicon wafers used as the substrate	[37]

Most of these techniques have disadvantages of being tedious, labor-intensive, sophisticated instrumentation, or costly reagents, which limit their practical applications [31]. However, in the present work, simple and cost effective methods have been designed for quick and sensitive determination of these purine compounds. Moreover, this fluorescence turn off – turn on technique can be used for both qualitative as well as quantitative detection of these anti-cancer drugs.

CHAPTER 3

METHODOLOGY

3.1 Materials and Reagents

All reagents used were of analytical reagent grade and were used without any advanced refinement. Ascorbic acid (99%, lobachemie) was used without further purification. Kollicoat-IR (MW 45000Da) was gifted from BASF which was used as stabilizing agent in the synthesis of CQDs. Potassium permanganate and potassium chloride purchased from CDH private limited were used to synthesize the manganese dioxide NS and NF. Ultrapure deionized water obtained from Millipore (Resistance: 18 MΩ) was used for preparation of all reagents and cleaning of glass wares.

3.2 Synthesis of Carbon Quantum Dots

Water soluble CQDs were synthesized by dissolving ascorbic acid and kollicoat (1:1, w/w%) with continuous stirring. After 30 minutes, the sample (5 mL) was transferred into a glass reaction vessel and subjected to microwave heating at 130^{o}C for 30 minutes at 300 W power with a Multiwave-3000 microwave reaction system (Anton Paar, USA). The formation of CQDs was confirmed with the change in the color of sample from colorless to pale yellow.
The scheme for the synthesis of CQDs has been illustrated in Figure 3.1.

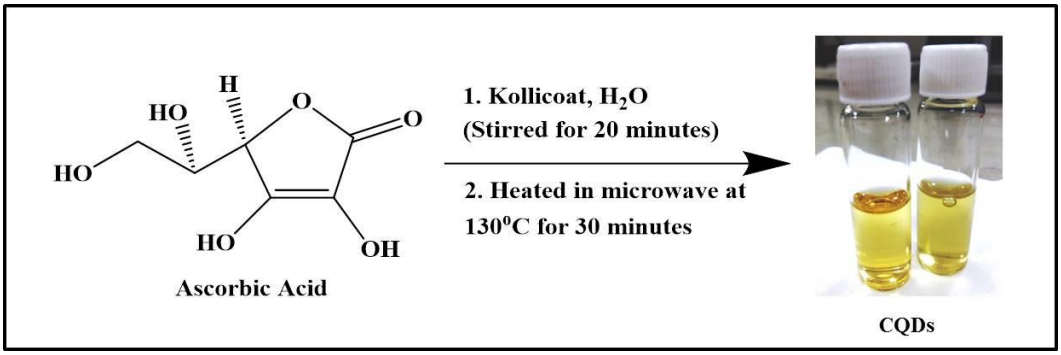

Figure 3.1 Scheme for the Synthesis of CQDs.

3.3 Synthesis of MnO_2Nanoflowers and Nanosheets

The hydrothermal method was used to prepare the MnO_2 NF and NS. At first, $KMnO_4$ and KCl were dissolved in 40 mL distilled water in different parts (n($KMnO_4$):n(KCl) = 3:1 and 1:3). The aqueous solutions were stirred continuously for 10 minutes to mix at room temperature. A 50 mL Teflon-lined stainless-steel autoclave was taken and the resultant solution was transferred into it followed by heating to 160^{o}C for 12 h. The autoclave was

eventually cooled down to the room temperature. The dark precipitates finally obtained were used after washing with distilled water and ethanol thoroughly and drying at 60^{o}C for 12 h.

3.4 Instrumentation

Electronic excitations of CQDs and MnO_2 NF and NS were analysed using a UV-Vis spectrophotometer (Analytik Jena, Specord, India) and fluorescence spectrophotometer (PerkinElmer LS-55, USA) using an excitation wavelength ranging from 260-320 nm. The XPS spectra of the catalysts were measured using XPS spectrometer (KRATOS Axis 165, Shimadzu, UK) with Mg Kα radiation 1253.6 eV at 75 W. The morphology and composition as synthesized MnO_2 NF were analyzed by scanning electron microscope, transmission electron microscope and Oxford INCTA energy dispersive X-ray (EDX) spectrometer. Phase identification was made with a X-ray diffractometer (PanalyticalX'Pert PRO, India) using Cu Kα (λ = 1.540 Å) as the radiation source. Particle size distribution and zeta potential was determined by dynamic light scattering method (DLS, Zetasizer, Malvern). The surface area of these NS and NF were compared through BET surface area analyser of Autosorb-1, Quanta chrome instruments, USA.

3.5 Detection Procedure

For the detection of 6-TG and 6-MP, different concentrations of respective moieties were mixed with 46 mM MnO_2@CQDs' solution in a series of 3 mL glass cuvettes. The FL spectra were obtained after shaking for one minute at room temperature.

CHAPTER 4

RESULTS AND DISCUSSION

4.1 Characterization of Carbon Quantum Dots and MnO_2 Nanostructures

The UV-Vis absorption of CQDs and MnO_2 NF and NS were studied to investigate their optical properties. The UV-Visible absorption spectra of CQDs displayed in Figure 4.1.1 showed two absorption bands (λ_{max}) at 245 nm and 350 nm plausible due to $\pi \rightarrow \pi^*$ transition of the C = C bond and $n \rightarrow \pi^*$ transition of the C = O respectively [38]. The UV-Visible absorption spectra of MnO_2 NF and NS displayed in Figure 4.1.1 showed two absorption bands λ_{max}at 214 nm and 275 nm.

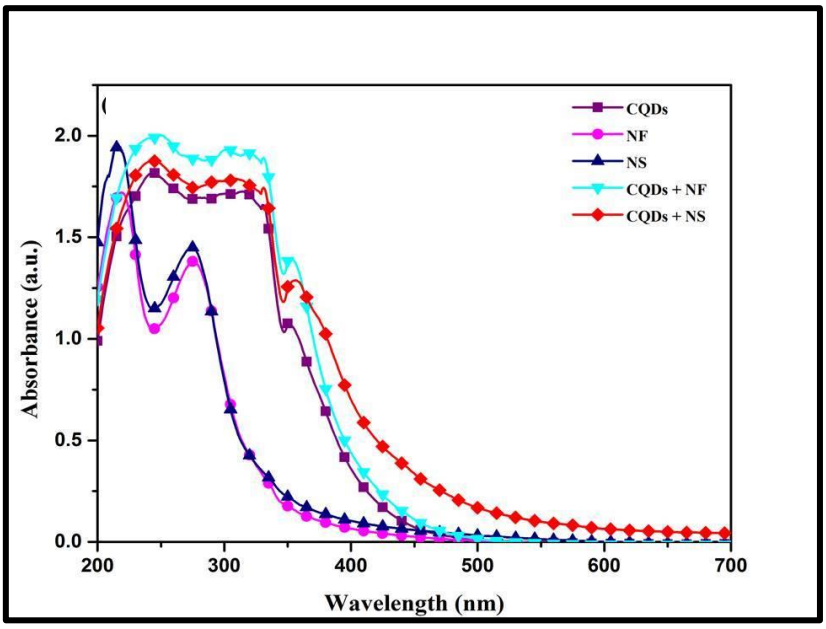

Figure 4.1.1 UV-Visible Absorption Spectra of CQDs, MnO_2 NF, MnO_2 NS, CQDs@NF and CQDs@NS.

The emission spectrum of CQDs at different excitation wavelengths is shown in Figure 4.1.2.

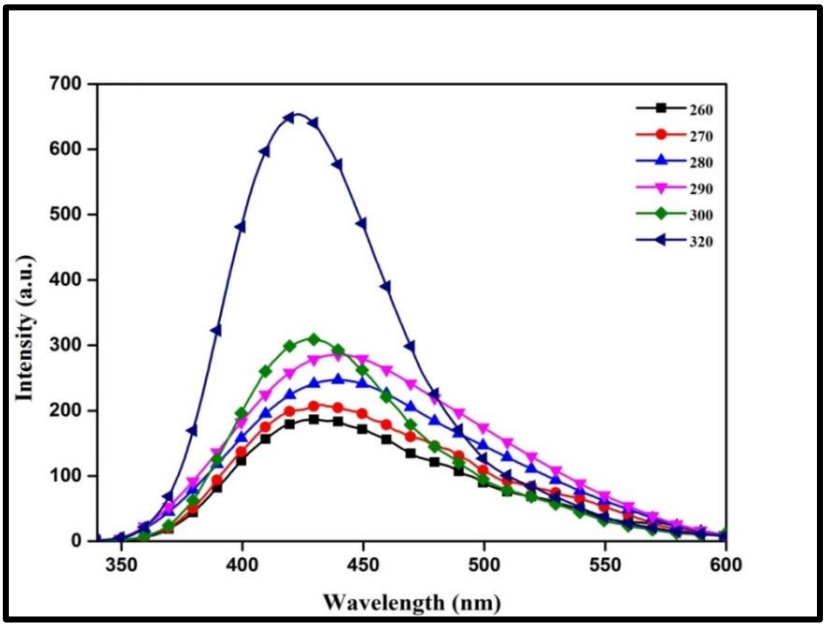

Figure 4.1.2 Emission Spectrum of CQDs at different Excitation Wavelengths.

X-Ray diffraction patterns of NF (Figure 4.1.3) show that the NF could be wellindexed to tetragonal MnO_2 as per the reference data JCPDS 24-0735.

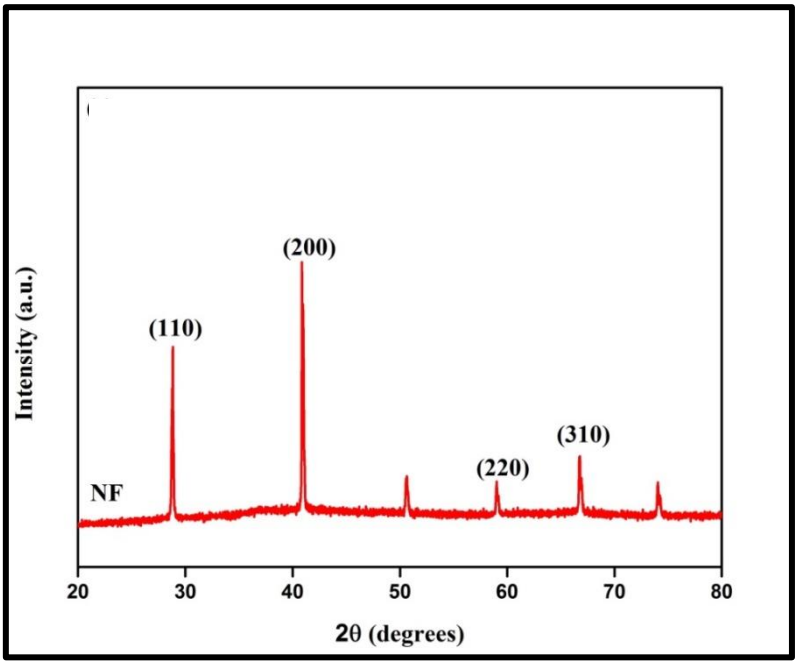

Figure 4.1.3 XRD Spectra of MnO_2 NF.

The MnO_2 NS were found to have greater surface area, pore volume and pore diameter than MnO_2 NF as shown in Table 4.1. Figure 4.1.4 represents the BET N_2adsoprtion-desorption curves for MnO_2 NF and NS. These curves exhibited the Type-II classification which depict that these show large deviations from Langmuir model of Adsorption and the intermediate flat region corresponds to monolayer formation [39].

Table 4.1 Comparison of MnO_2 NF and NS through BET Surface Area Analyser.

Nanostructures	Surface Area (m^2 g^{-1})	Pore volume (cm^3 g^{-1})	Pore diameter (nm)
NF	10.6	0.058	21.32
NS	11.1	0.059	22.16

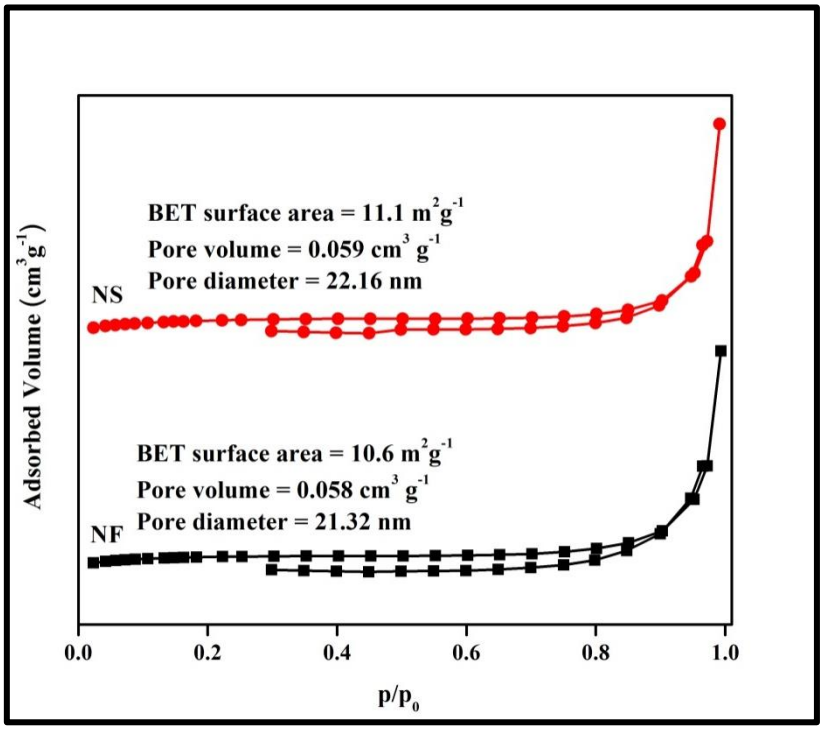

Figure 4.1.4 BET N_2 Adsorption–Desorption Curves for MnO_2 NF and NS.

The average hydrodynamic size has been found to be 7 nm for CQDs (Figure 4.2(a)). While the participation of MnO_2nanostructuresleads to agglomeration resulting in the increase of the size distribution up to 7.6 nm (Figure 4.2(b) and Figure 4.2(c)).

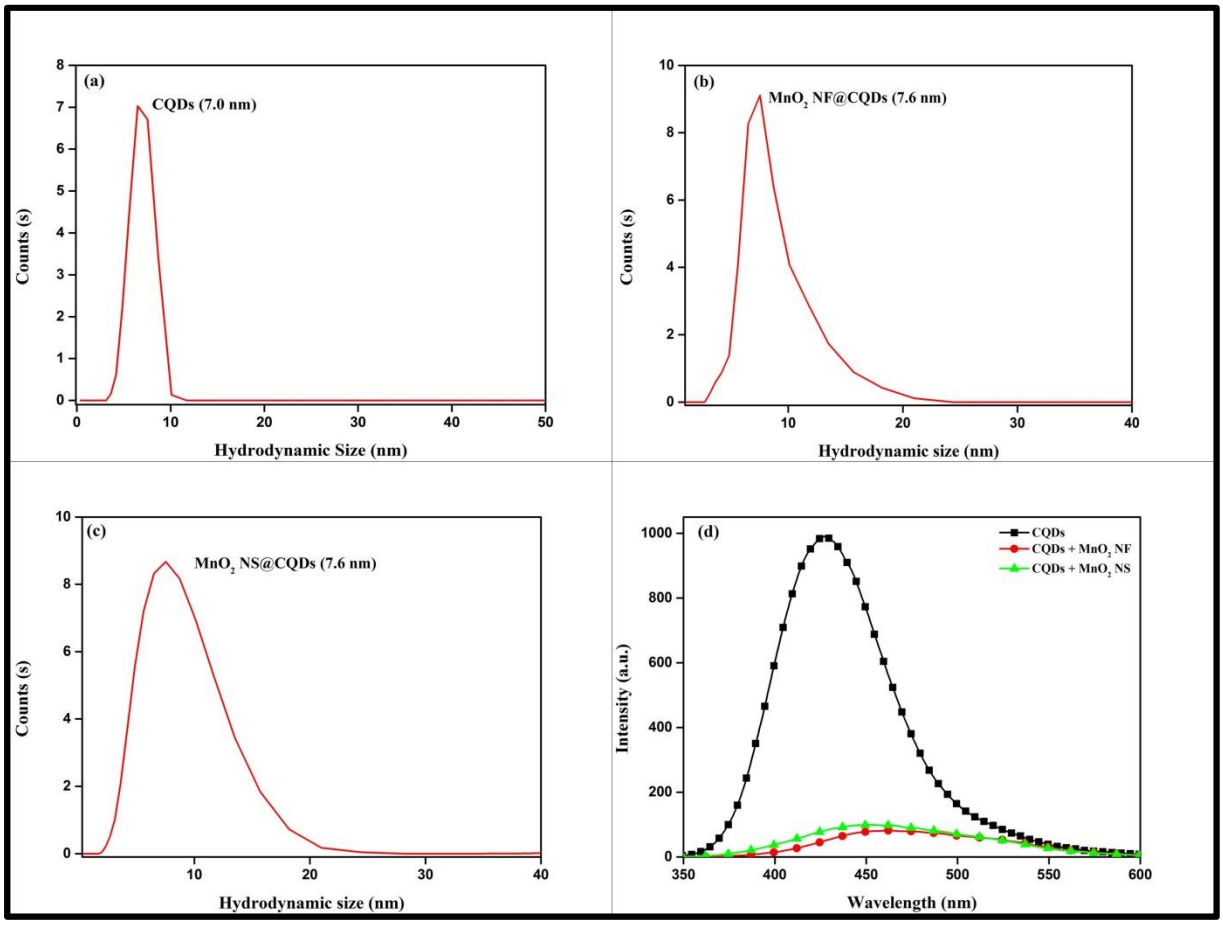

Figure 4.2 DLS Spectra for (a) CQDs, (b) MnO_2 NF@CQDs, (c) MnO_2 NS@CQDs, (d)Emission Spectrum of CQDs, MnO_2 NF@CQDs and MnO_2 NS@CQDs

The zeta potential value for CQDs, MnO_2 NF@CQDs and MnO_2 NS@CQDs were observed to be -0.912 mV, -2.24 mV and -0.141 mV respectively which confirm the negative charge on their surfaces.

XPS measurements were performed to determine the composition of CQDs. As shown in Figure 4.3.1 and Figure 4.3.2, the C 1s (285.31 eV) and O 1s (532.97 eV) peaks are the two major elements observed for CQDs.

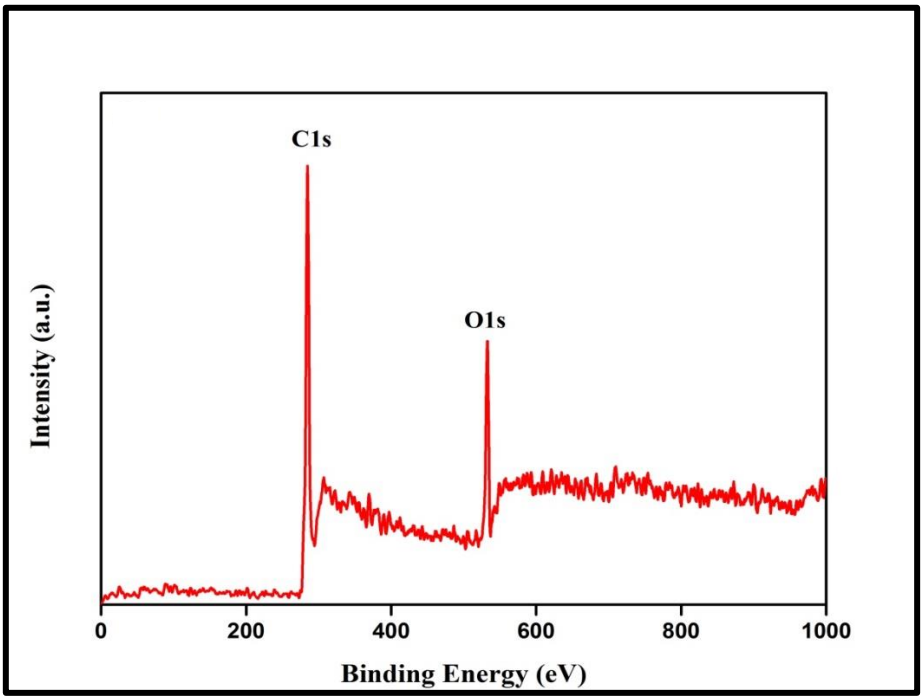

Figure 4.3.1 XPS Survey of CQDs.

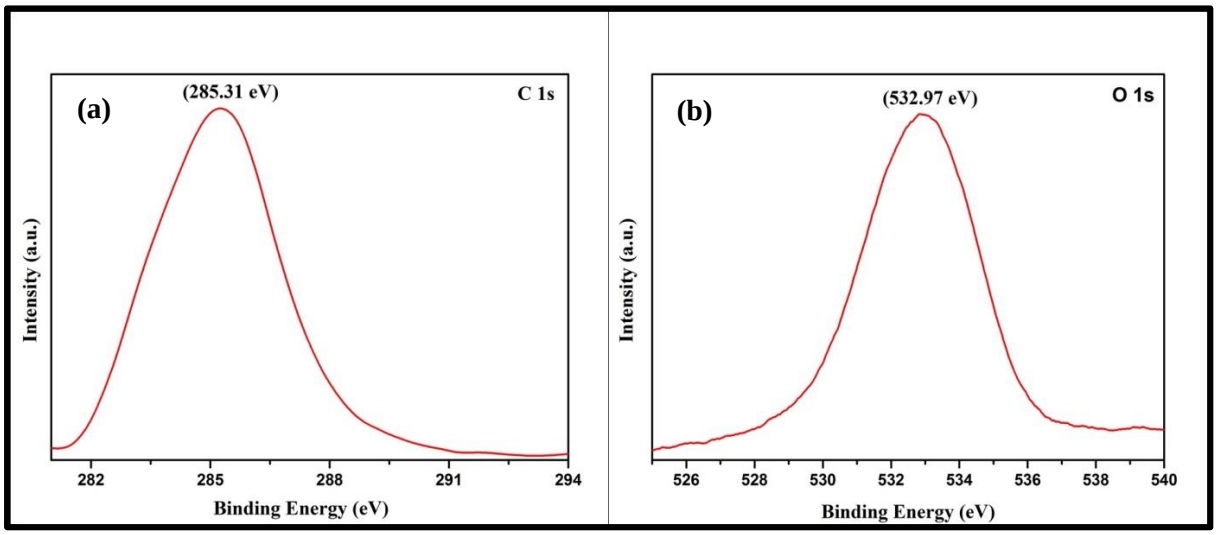

Figure 4.3.2 (a) C 1s and (b) O 1s Spectrum of CQDs.

The surface morphology and distribution of MnO_2 nanostructures over CQDs have been determined by HRTEM, SEM,EDS analysis and color mapping. The SEM observations (Figure 4.4), EDS analysis (Figure 4.5) clearly display the successful formation of MnO_2 nanostructures. The HRTEM image of MnO_2NF (Figure 4.7) displays the flower structures of MnO_2, Figure 4.6 displays MnO_2 NS images with lattice spacing of 0.40 nm. Moreover, the attainment of the CQDs – MnO_2 composite is observed in elemental mapping (Figure 4.8), which clearly shows that the CQDs are well combined on the surface of MnO_2 nanostructures.

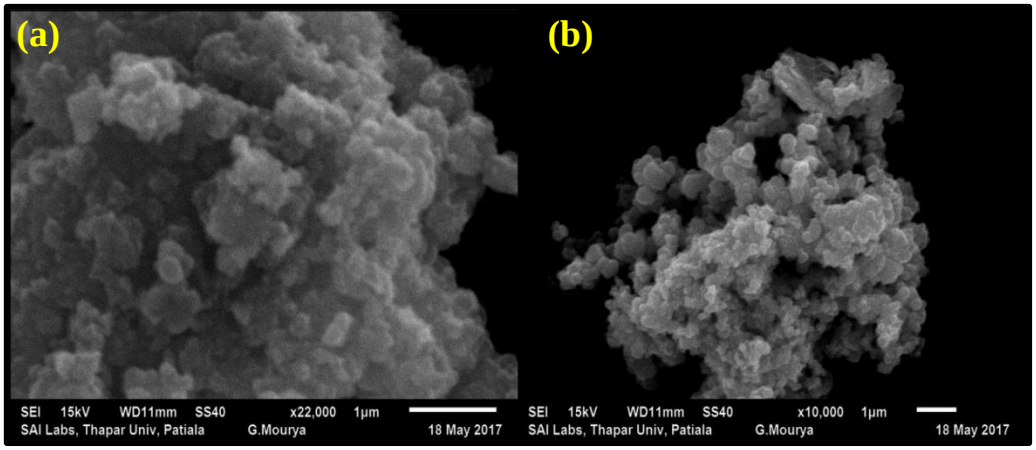

Figure 4.4 SEM images of MnO_2 NF at different magnifications.

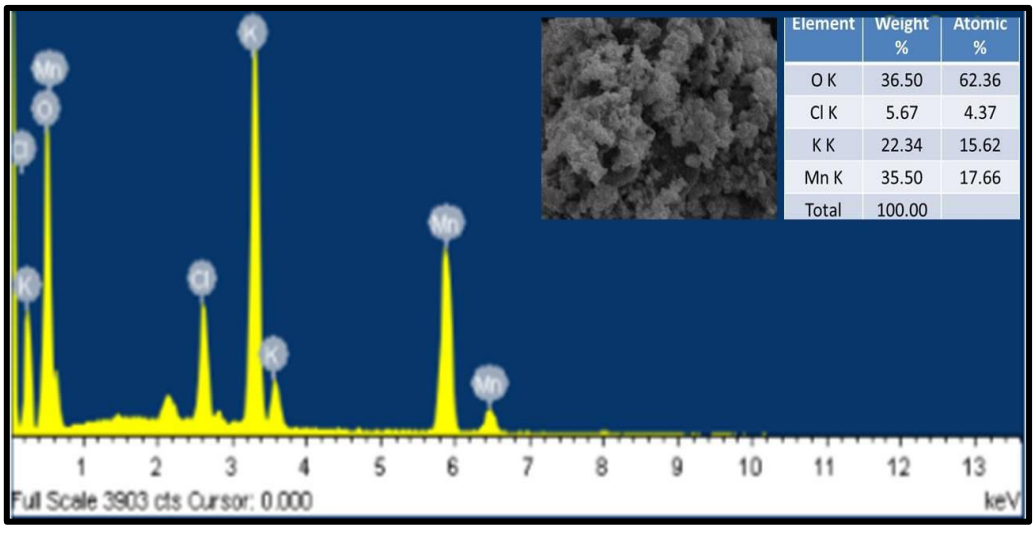

Figure 4.5 EDS of MnO_2 NF.

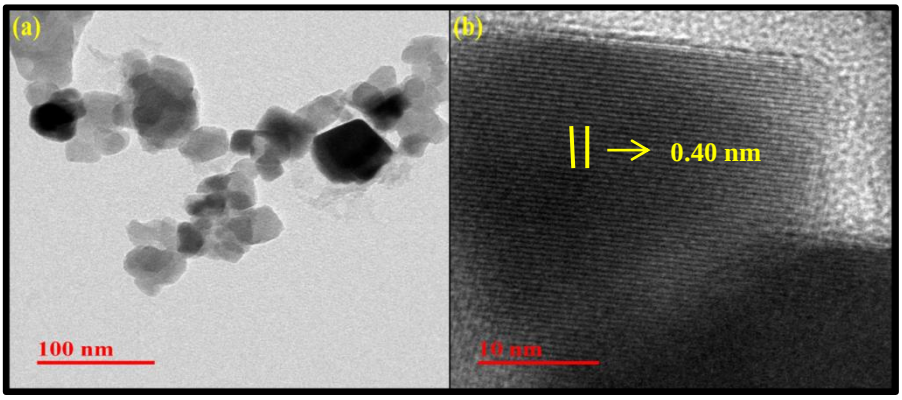

Figure 4.6 HRTEM images of MnO_2 NS.

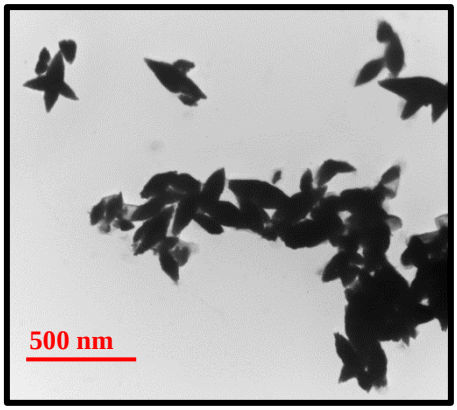

Figure 4.7 HRTEM image of MnO_2 NF.

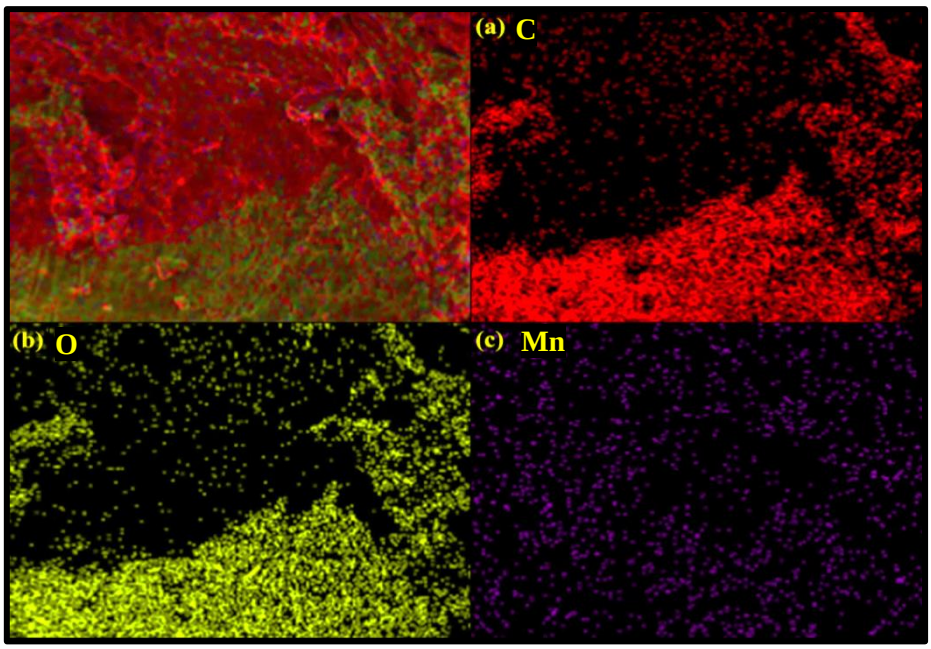

Figure 4.8 Elemental Mapping of MnO_2 NF@CQDs for (a) C, (b) O and (c) Mn.

4.2 Fluorescence Turn-Off of Carbon Quantum Dots by MnO_2 Nanostructures

The confirmation for the reduction of MnO_2 by CQDs was observed by the fluorescence quenching. Initially the CQDs showed very high fluorescence which is attributed to the radiative recombination of electrons and to the confinement of holes over the surface of these CQDs. By the interaction of CQDs with MnO_2,the electrons and holes are trapped and thus, they become less available for the radiative recombination which ultimately leads to PL quenching. With the increasing concentration of MnO_2 NF and NS, the fluorescence intensity of CQDs decreases considerably, demonstrating an efficient quenching procedure Fluorescence quenching data are usually represented by Stern-Volmer equation which gives the plot between F_0/F vs. concentration of the quencher and is represented as:

$$\mathbf{F_0/F = 1+K_{SV}\,[Q]}$$

Here, 'F' and 'F_0' are the fluorescence intensity of CQDs in the presence and absence of quencher [Q], 'K_{SV}'is the Stern-Volmer constant (M^{-1}) [17]. The plot is represented in Figure 4.9.1 and Figure 4.9.2 and the corresponding value of K_{SV} is calculated to be 2.8×10^{-4} M^{-1} for NF and 1.9×10^{-4} M^{-1} for NS indicating high quenching efficiency.

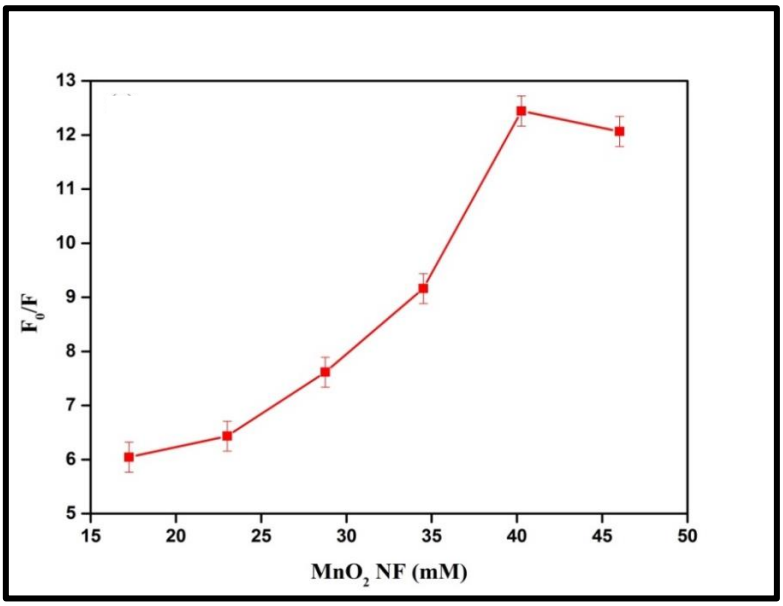

Figure 4.9.1 Stern-Volmer Plot for the Quenching of CQDs Fluorescence at various concentrations of MnO_2 NF.

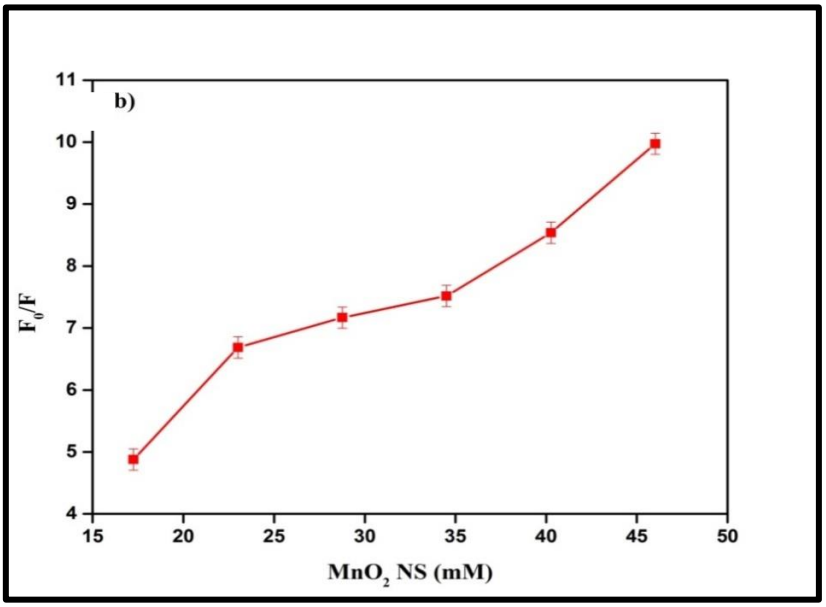

Figure 4.9.2 Stern-Volmer Plot for the Quenching of CQDs Fluorescence at various concentrations of MnO_2 NS.

4.3 Photostability of Carbon Quantum Dots

Before carrying out the practical application for the sensing of 6-TG and 6-MP, the stability of CQDs was done by the UV (125 W Hg arc) and visible light (CFL 60 W) irradiation for 60 minutes and no change was observed in the fluorescence intensity signifying the good photostability.

4.4 Kinetic Study (Testing at Different Time Intervals)

The fluorescence intensity decreased significantly with increase in the incubation time. The kinetic study was performed for MnO_2 NF and NS upto the incubation time of 12 h as shown in Figure 4.10.1 & Figure 4.10.2. 12 h was selected as optimum time for the interaction of MnO_2 NF and NS with CQDs which remains stable afterwards.

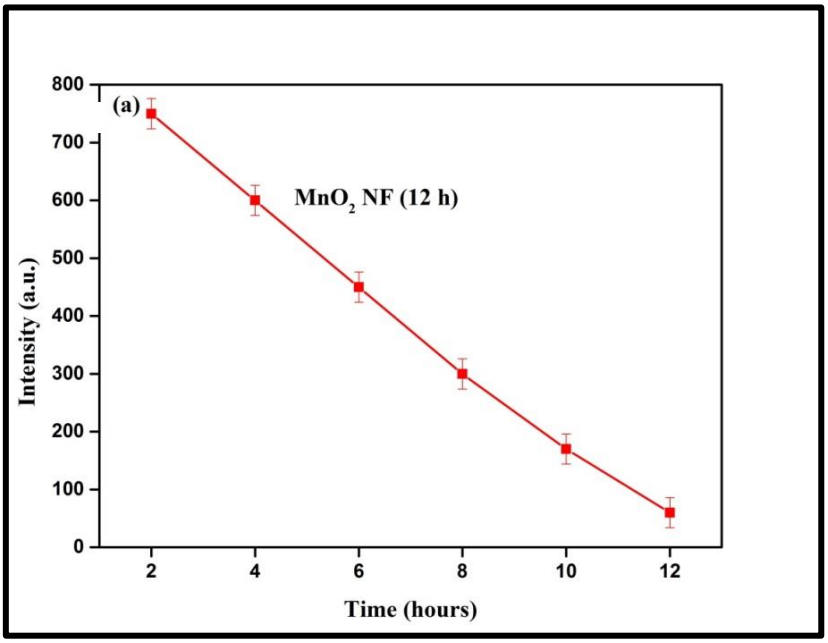

Figure 4.10.1 Kinetic study to optimize time for the interaction of MnO_2 NF (12 h).

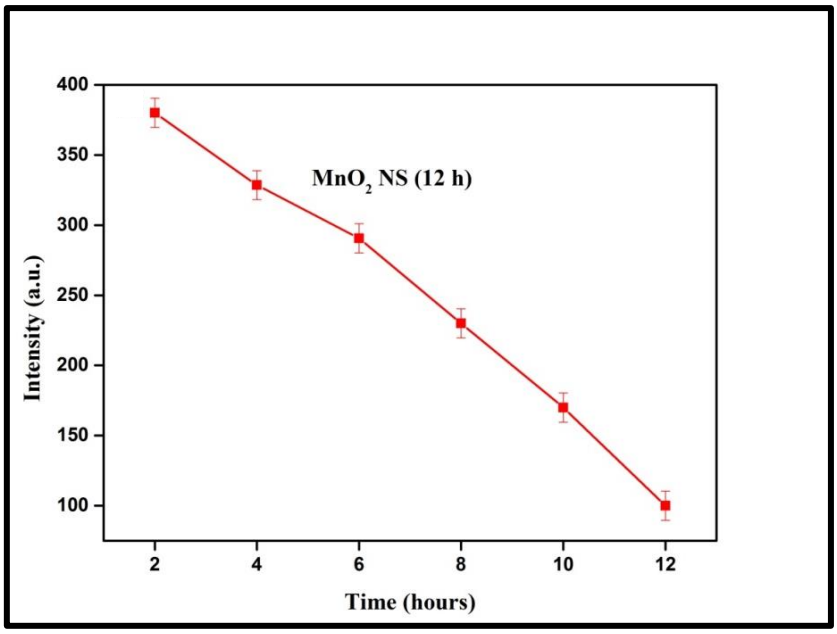

Figure 4.10.2 Kinetic study to optimize time for the interaction of MnO_2 NS (12 h).

4.5 Fluorescence Turn-On Detection of 6-TG

On addition of 6-TG, both, MnO_2 NF and NS, exhibit turn-on behaviour in fluorescence. There was no change in the fluorescence intensity and position of the peak of CQDs on addition of 6-TG to the CQDs solution, which indicates that two of these did not interact. The MnO_2 NF@CQDs and NS@CQDs exhibit fluorescence turn-on property on adding 20 mL6-

TG at each time as shown in Figure 4.11.1 & Figure 4.11.2 respectively, which indicated that with the small addition (20 μL) of 6-TG even, significant change in the fluorescence intensity was observed.

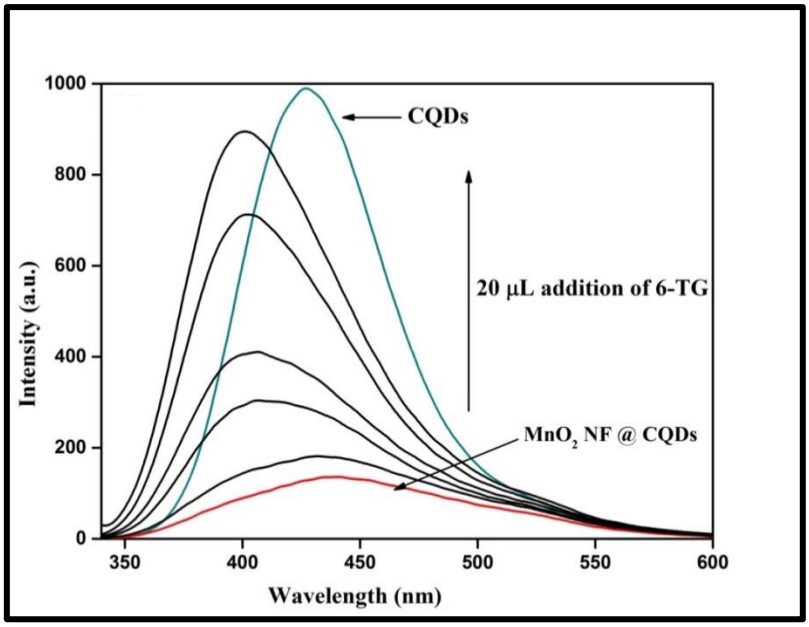

Figure 4.11.1 Emission Spectrum of MnO_2 NF@CQDs after addition of different concentrations of 6-TG.

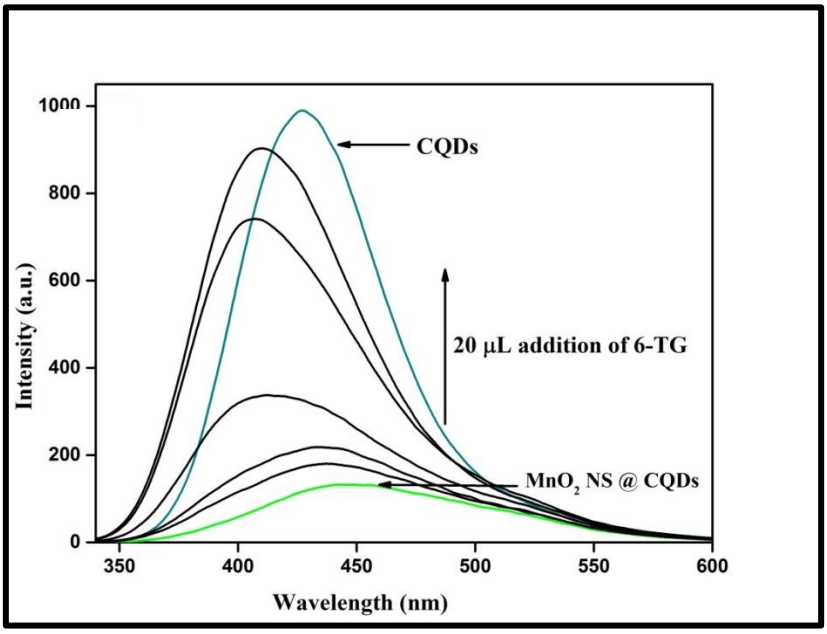

Figure 4.11.2 Emission Spectrum of MnO_2 NS@CQDs after addition of different concentrations of 6-TG.

An exponential relationship between the (F/F_0) against the concentration of 6-TG was also obtained in the range of 0-50 μM with the correlation coefficient of 0.9961 with MnO_2 NF (Figure 4.12.1) and 0.9917 with MnO_2 NS (Figure 4.12.2). This fluorescence turn-on

behaviour was due to the interaction of 6-TG with MnO_2 nanostructures via Mn-S bond, which leads to aggregation of nanostructures. The detection limit (3σ/s) for 6-TG was found to be 0.015 µM with NF and 0.015 µM for NS, where 'σ' represents the standard deviation of five blank measurements, and 's' is the slope of the calibration curve.

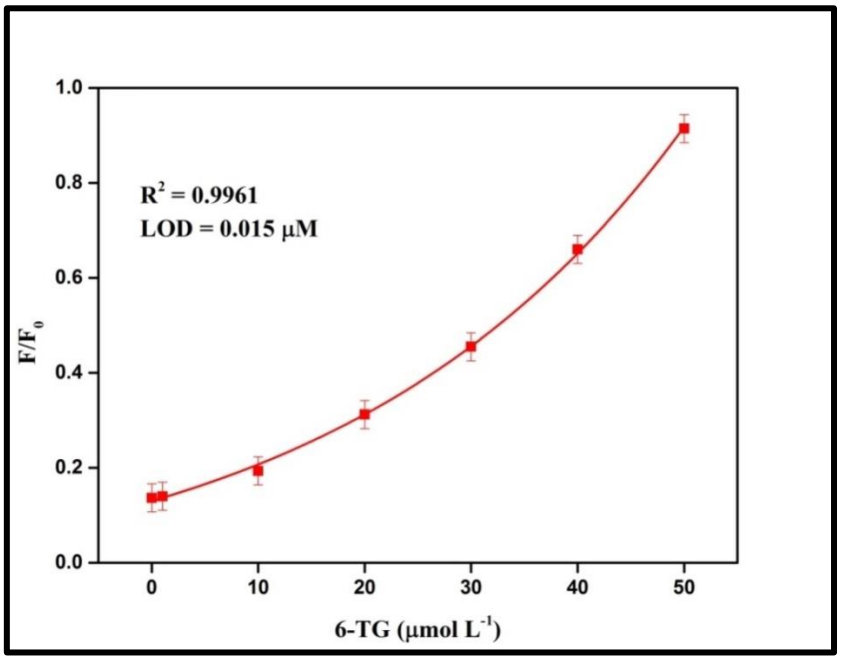

Figure 4.12.1 Exponential relationship between the F/F_0 against the concentration of 6-TG in the range 0-50 µM with the Correlation Coefficient of 0.9961.

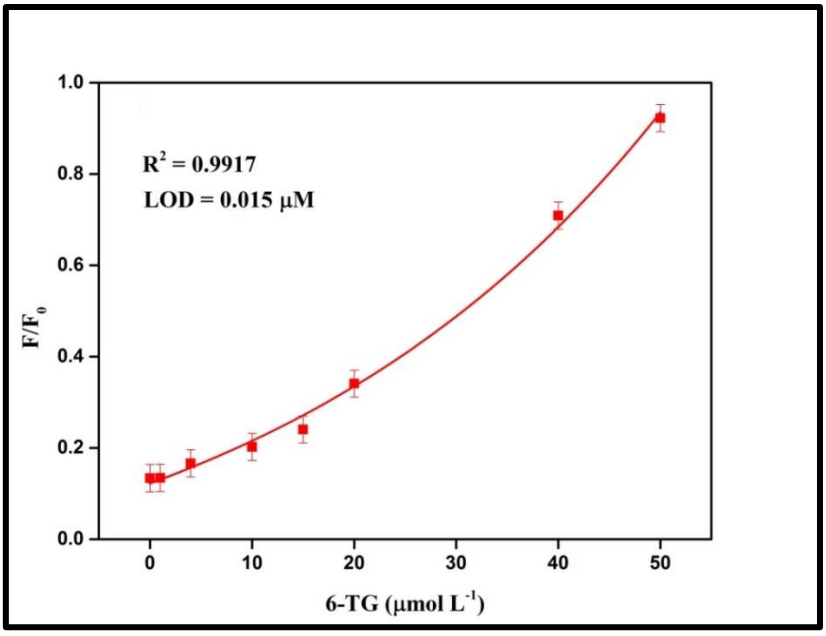

Figure 4.12.2 Exponential relationship between the F/F_0 against the concentration of 6-TG in the range 0-50 µM with the Correlation Coefficient of 0.9917.

4.6 Fluorescence Turn-On Detection of 6-MP

On addition of 6-MP, both, MnO_2 NF and NS, exhibit turn-on behaviour in fluorescence. There was no change in the fluorescence intensity and position of the peak of CQDs on addition of 6-MP to the CQDs solution, which indicates that two of these did not interact. The MnO_2 NF@CQDs and NS@CQDs exhibit fluorescence turn-on property on adding 20 mL6-MP at each time as shown in Figure 4.13.1 & Figure 4.13.2 respectively, which indicated that even with the small addition (20 μL) of 6-MP considerable change in the fluorescence intensity was observed.

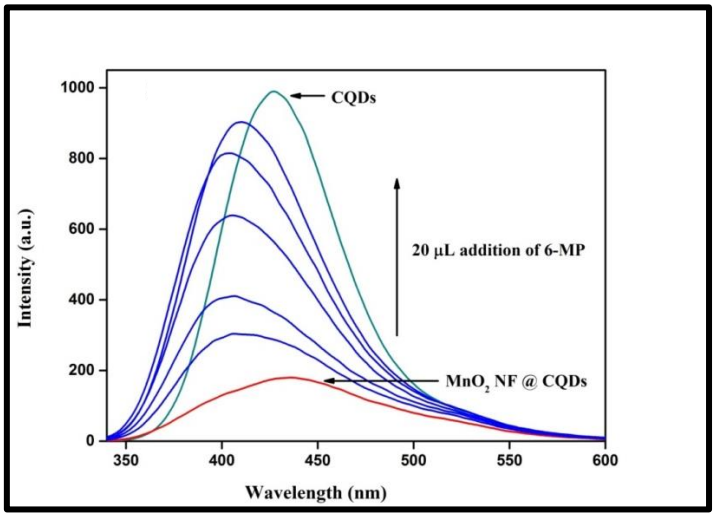

Figure 4.13.1 Emission Spectrum of MnO_2 NF@CQDs after addition of different concentrations of 6-MP.

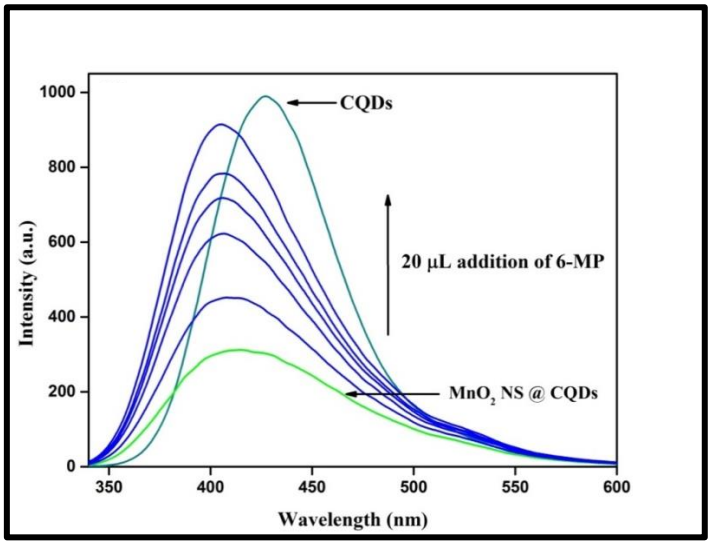

Figure 4.13.2 Emission Spectrum of MnO_2 NS@CQDs after addition of different concentrations of 6-MP.

An exponential relationship between the (F/F_0) against the concentration of 6-MP was also obtained in the range of 0-50 µM with the correlation coefficient of 0.9945 with MnO_2 NF (Figure 4.14.1) and 0.9989 with MnO_2 NS (Figure 4.14.2). This fluorescence turn-on behaviour was due to the interaction of 6-MP with MnO_2 nanostructures via Mn-S bond, which leads to aggregation of nanostructures. The detection limit (3σ/s) for 6-MP was found to be 0.014 µM with NF and 0.012 µM for NS, where 'σ' represents the standard deviation of five blank measurements, and 's' is the slope of the calibration curve.

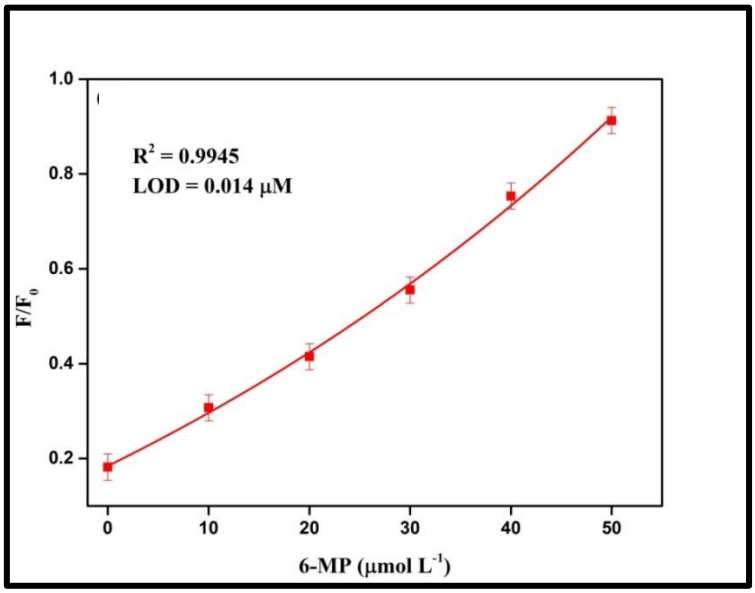

Figure 4.14.1 Exponential relationship between the F/F_0 against the concentration of 6-MP in the range 0-50 µM with the Correlation Coefficient of 0.9945.

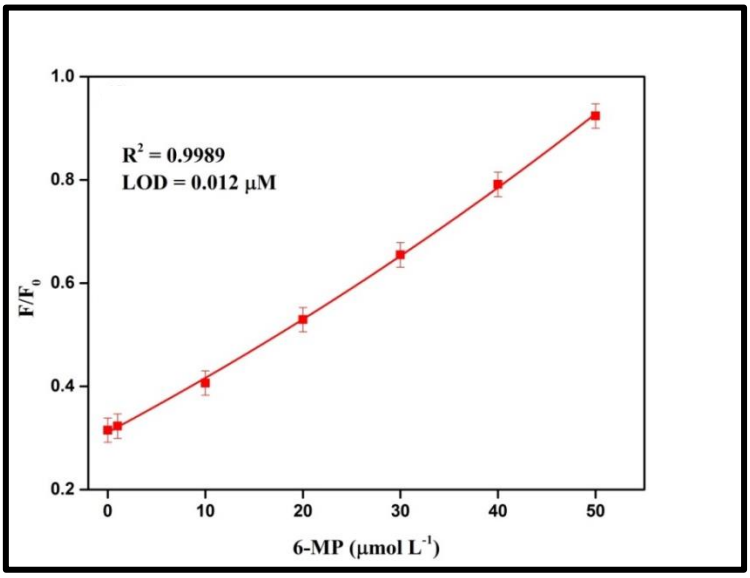

Figure 4.14.2 Exponential relationship between the F/F_0 against the concentration of 6-MP in the range 0-50 µM with the Correlation Coefficient of 0.9989.

4.7 Mechanism for Fluorescence Turn Off - Turn On Detection of 6-TG and 6-MP by Carbon Quantum Dots

As shown in Figure 4.2(d) the fluorescence intensity of CQDs was quenched by 93% with the interaction of MnO_2forming MnO_2 NF@CQDs and NS@CQDs. The quenching of fluorescence exhibited by CQDs due to MnO_2 nanostructures is mainly plausible because of Fluorescence Resonance Energy Transfer (FRET) phenomenon. This quenching behavior may also be due to the electron-transfer and inner-filter effect [33]. As shown in Figure 4.15, the fluorescence emission spectrum of CQDs (λ_{em} = 420 nm) overlap with the absorption spectrum of MnO_2 nanostructures (λ_{max}= 275 nm). As inferred from the observations, a FRET mechanism is likely to occur in the MnO_2-CQDs probe where CQDs act as donor and MnO_2 nanostructures act as acceptor. Consequently, effective quenching of CQDs' fluorescence takes place. However, on addition of 6-TG and 6-MP, the Mn-S bond is expected to form which leads to regaining of fluorescence intensity of CQDs.

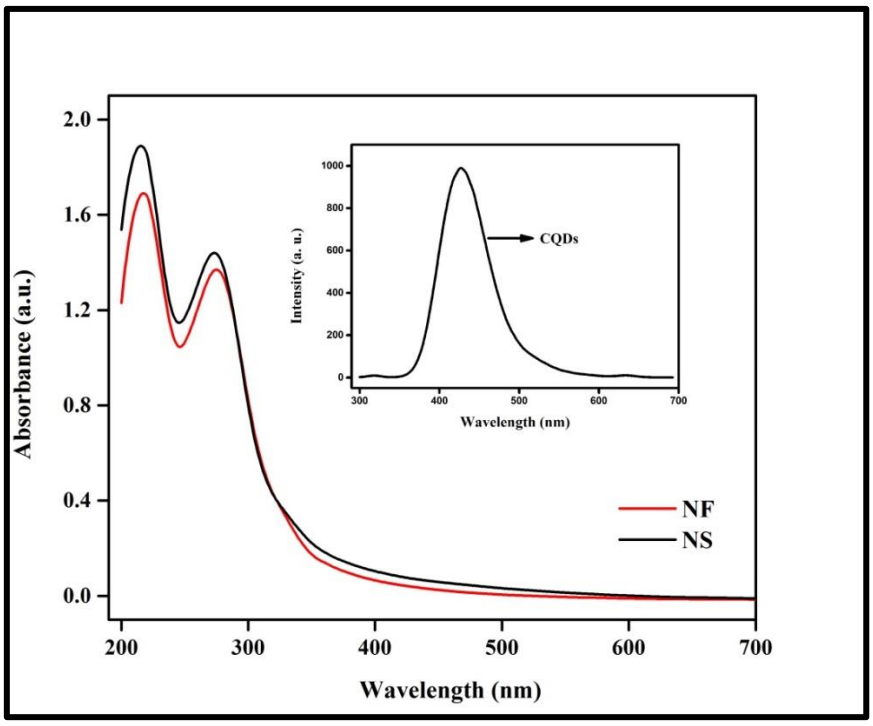

Figure 4.15 Overlap of Absorption Spectrum of MnO_2 Nanostructures with the Emission Spectrum of CQDs (inset).

The principle of the method is explained in Figure 4.16.

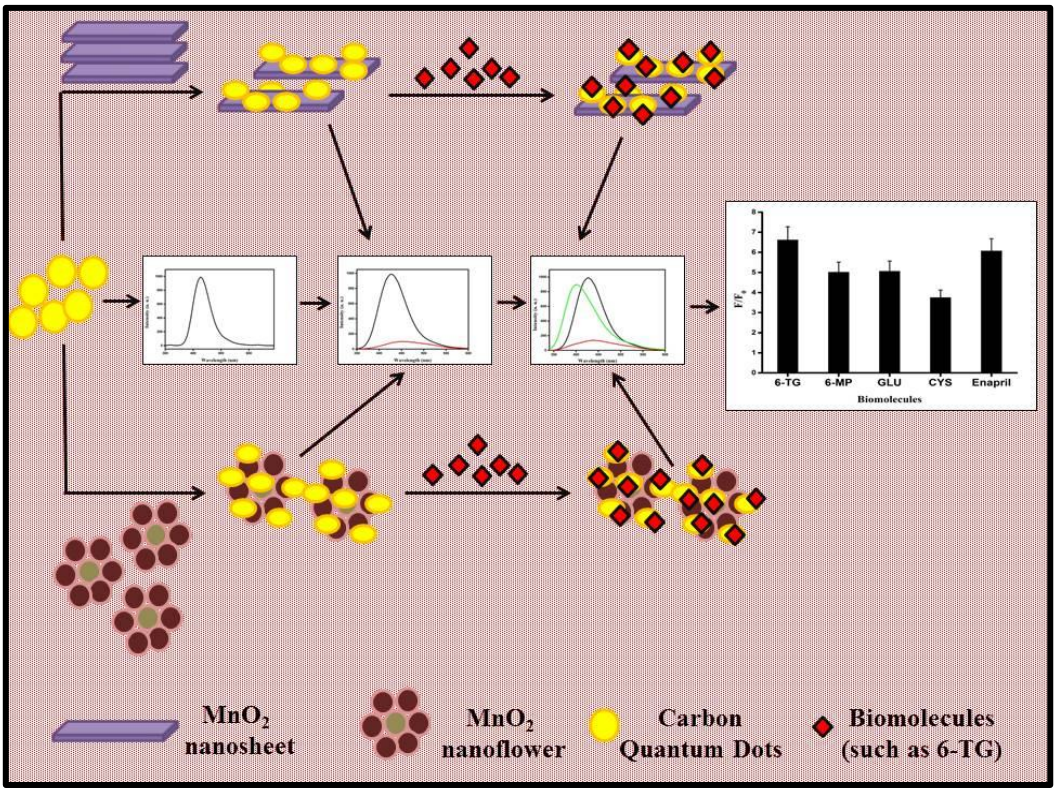

Figure 4.16 Proposed Mechanism for Fluorescence Turn Off – Turn On of CQDs.

4.8 Analytical Application

To promote the relevance and applicability of MnO_2@CQDs as biosensor for pharmaceutical utility and in biological industries, the whole scheme was performed for several biomolecules and Enapril tablets. Enapril tablets contain Enalapril Maleate as an active ingredient and are generally used for treating high blood pressure and heart failure. The results recommended that the MnO_2@CQDs composite is suitable for thiol containing biomolecules, as shown in Figure 4.19. The amino acids which do not contain free thiol groups aren't capable of exchanging the CQDs from the surface of MnO_2 nanostructures. The enhanced fluorescence intensity with the addition of 20 μL Enapril at each time is as shown in Figure 4.17.1 and Figure 4.17.2.

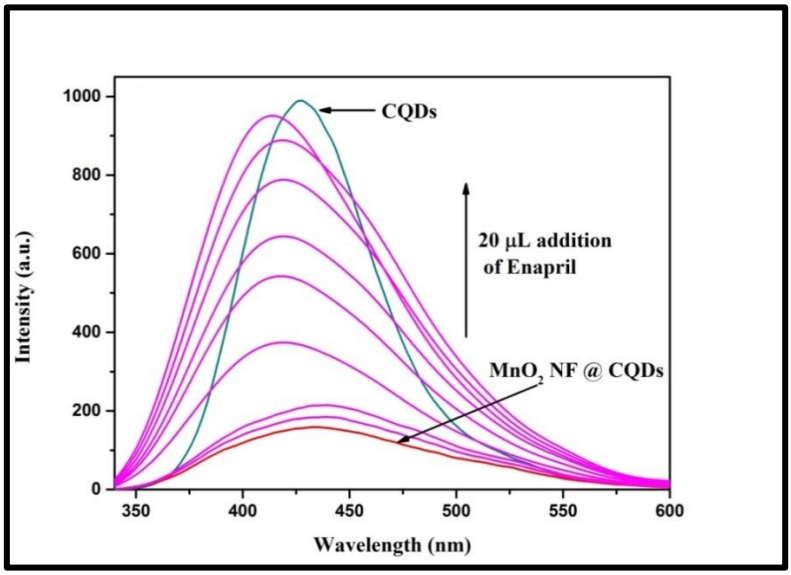

Figure 4.17.1 Emission Spectrum of MnO_2 NF@CQDs after addition of different concentrations of Enapril.

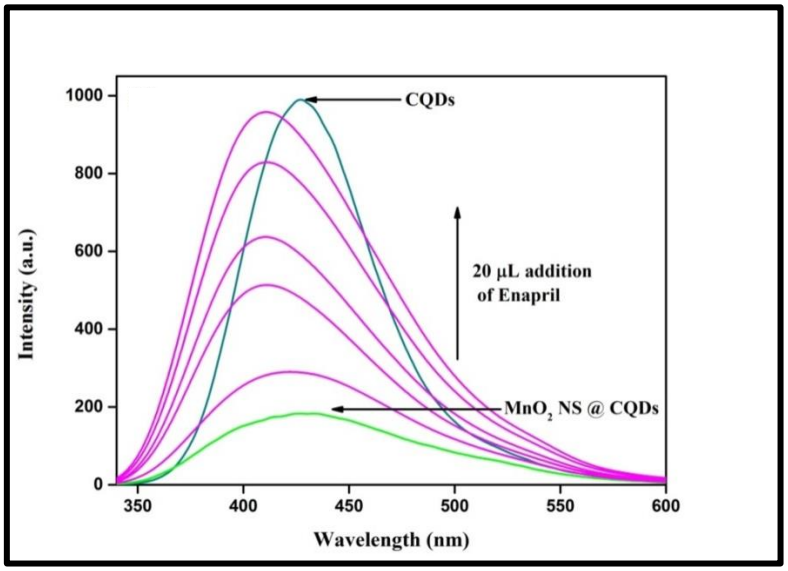

Figure 4.17.2 Emission Spectrum of MnO_2 NS@CQDs after addition of different concentrations of Enapril.

The turn-on fluorescence is linearly dependent upon the concentration of enapril with correlation coefficient of 0.9917 and observed LOD is 0.016 µM (Figure 4.18.1) for MnO_2 NF. Similarly, the turn on fluorescence is linearly dependent upon the concentration of enapril with correlation coefficient of 0.9909 and observed LOD is 0.011 µM (Figure 4.18.2) for MnO_2 NS.

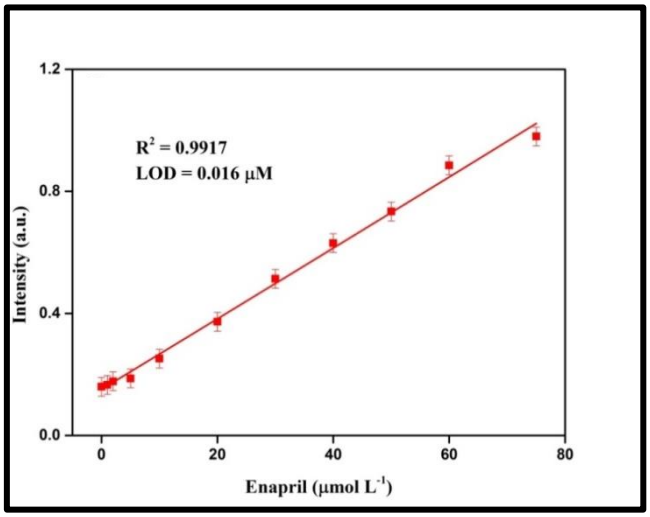

Figure 4.18.1 Exponential relationship between the F/F_0 against the concentration of Enapril in the range 0-50 µM.

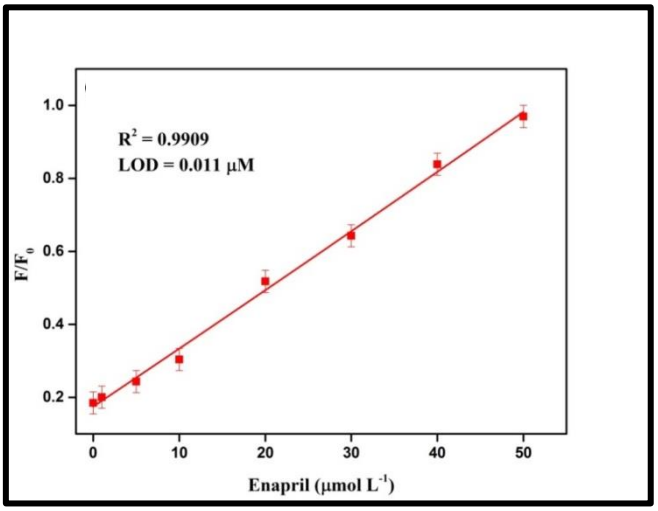

Figure 4.18.2 Exponential relationship between the F/F_0 against the concentration of Enapril in the range 0-50 µM.

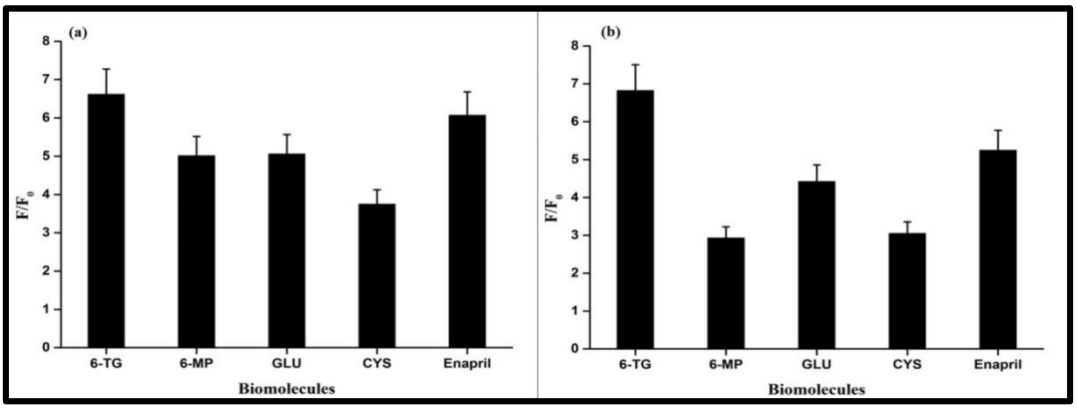

Figure 4.19 Comparison of F/F_0 values for different biomolecules with (a) MnO_2 NF@CQDs and (b) MnO_2 NS@CQDs.

Comparatively, this method is better than those previously reported techniques and biosensors (Table 4.2 and Table 4.3). This suggests that the composite is highly beneficial for the usage as a fluorescence sensor for thio-biols.

Table 4.2 A Comparative Study for the Performance of Optical Sensors for 6-Thioguanine.

Biosensor	Method	Linear Range (μM)	LOD (μM)	Reference
Gold nanorod	LSPR	0.02 – 1.0	0.015	[28]
Gold nanosphere	LSPR	0.05 – 0.5	0.022	[28]
Silver NPs	SERS	0.1 – 15.0	0.065	[37]
$[Co(bpy)_3]^{2+/3+}$	SWV	0.4 – 22	0.008	[26]
$[Fe(CN)_6]^{3-/4-}$	DPSV	1.1 – 11	0.2	[26]
Silver NPs	Fluorescence	0.015 – 0.75	0.009	[21]
MnO_2 NF	Fluorescence	0.0 – 50.0	0.015	Present Work
MnO_2 NS	Fluorescence	0.0 – 50.0	0.015	Present Work

Table 4.3 A Comparative Study for the Performance of Optical Sensors for 6-Mercaptopurine.

Biosensor	Method	Linear Range (μM)	LOD (μM)	Reference
MIP	Fluorescence	0.06 – 39.2	0.019	[33]
Multiwall carbon nanotubes	DPA	0.2 – 100	0.08	[36]
Gold NPs	Fluorescence	0.1 – 120	0.019	[34]
Gold NPs	Chemiluminescence	0.009 – 18	0.006	[40]
Silver NPs	Fluorescence	0.06 – 0.3	0.048×10^{-2}	[32]
MnO_2 NF	Fluorescence	0 –50	0.014	Present Work
MnO_2 NS	Fluorescence	0 – 50	0.012	Present Work

CHAPTER 5

CONCLUSION

In present work, we have successfully demonstrated the biosensor for the turn off – turn on fluorescence of CQDs. The CQDs were synthesized by the simplistic and cost-effective approach using ascorbic acid as precursor. The interaction of MnO_2 with CQDs leads to fluorescence quenching due to FRET mechanism where CQDs act as donor and MnO_2 nanostructures act as acceptor. The fluorescence intensity was regained by using 6-TG via formation of Mn-S bond. A thorough analysis into the development of fluorescence turn off - turn on of CQDs was done for enapril tablets which furnished positive response. This assay was also investigated for different other biomolecules to increase its utility in pharmaceutical industries. The proposed mechanism for the turn off – turn on fluorescence of CQDs was also elaborated in this work.

CHAPTER 6

REFERENCES

1. Africa, A.o.S.o.S., *Evidence-based Practice:'Double Symposium'proceedings on problems, possibilities and politics*. 2006: Academy of Science of South Africa.
2. Whitesides, G.M., *Nanoscience, nanotechnology, and chemistry.* Small, 2005. **1**(2): p. 172-179.
3. Pedersen, K., *Quantum size effects in nanostructures.* Organic and Inorganic Nanostructures, 2006.
4. Habiba, K., et al., *Fabrication of nanomaterials by pulsed laser synthesis.* Manufacturing Nanostructures, One Central Press, Manchester, UK, 2014.
5. Heiligtag, F.J. and M. Niederberger, *The fascinating world of nanoparticle research.* Materials Today, 2013. **16**(7): p. 262-271.
6. Ghaderi, S., *Development of fluorescent nanoparticles 'quantum dots' for biomedical application*. 2012, UCL (University College London).
7. Lim, S.Y., W. Shen, and Z. Gao, *Carbon quantum dots and their applications.* Chemical Society Reviews, 2015. **44**(1): p. 362-381.
8. Wang, Y. and A. Hu, *Carbon quantum dots: synthesis, properties and applications.* Journal of Materials Chemistry C, 2014. **2**(34): p. 6921-6939.
9. Qi, Y. and B. Li, *Spectr ochimica Acta Part A: Molecul ar and Biomo lecular Spectrosco py.* Spectrochimica Acta Part A: Molecular and Biomolecular Spectroscopy, 2013. **111**: p. 1-6.
10. Yan, X., et al., *A ratiometric fluorescent quantum dots based biosensor for organophosphorus pesticides detection by inner-filter effect.* Biosensors and Bioelectronics, 2015. **74**: p. 277-283.
11. Li, J., et al., *Fluorescence turn-on detection of glucose via the Ag nanoparticle mediated release of a perylene probe.* Chemical Communications, 2015. **51**(29): p. 6354-6356.
12. Yang, G., et al., *Graphene-like two-dimensional layered nanomaterials: applications in biosensors and nanomedicine.* Nanoscale, 2015. **7**(34): p. 14217-14231.
13. Yan, X., et al., *Graphene Quantum Dot–MnO2 Nanosheet Based Optical Sensing Platform: A Sensitive Fluorescence "Turn Off–On" Nanosensor for Glutathione Detection and Intracellular Imaging.* ACS applied materials & interfaces, 2016. **8**(34): p. 21990-21996.

14. Zhao, Z., et al., *Activatable fluorescence/MRI bimodal platform for tumor cell imaging via MnO2 nanosheet–aptamer nanoprobe.* Journal of the American Chemical Society, 2014. **136**(32): p. 11220-11223.
15. Chen, Y., et al., *Two-dimensional graphene analogues for biomedical applications.* Chemical Society Reviews, 2015. **44**(9): p. 2681-2701.
16. Deng, R., et al., *Intracellular glutathione detection using MnO2-nanosheet-modified upconversion nanoparticles.* Journal of the American Chemical Society, 2011. **133**(50): p. 20168-20171.
17. Lakowicz, J.R. and B.R. Masters, *Principles of fluorescence spectroscopy.* Journal of Biomedical Optics, 2008. **13**(2): p. 029901.
18. Lakowicz, J., *Principles of fluorescence spectroscopy Kluwer Academic Plenum.* New York, 1999.
19. Harms, D. and G. Janka-Schaub, *Co-operative study group for childhood acute lymphoblastic leukemia (COALL): long-term follow-up of trials 82, 85, 89 and 92.* Leukemia, 2000. **14**(12): p. 2234.
20. Zakrzewski, R., *Application of the iodine–azide postcolumn reaction in RP‐HPLC for the determination of thioguanine in urine.* Journal of separation science, 2008. **31**(12): p. 2199-2205.
21. Amjadi, M. and L. Farzampour, *Selective turn‐on fluorescence assay of 6–thioguanine by using harmine‐modified silver nanoparticles.* Luminescence, 2014. **29**(6): p. 689-694.
22. Lavi, L.E. and J.S. Holcenberg, *A rapid and sensitive high-performance liquid chromatographic assay for 6-mercaptopurine metabolites in red blood cells.* Analytical biochemistry, 1985. **144**(2): p. 514-521.
23. Keuzenkamp-Jansen, C., et al., *Determination of extracellular and intracellular thiopurines and methylthiopurines by high-performance liquid chromatography.* Journal of Chromatography B: Biomedical Sciences and Applications, 1995. **672**(1): p. 53-61.
24. Lennard, L. and H.J. Singleton, *High-performance liquid chromatographic assay of the methyl and nucleotide metabolites of 6-mercaptopurine: quantitation of red blood cell 6-thioguanine nucleotide, 6-thioinosinic acid and 6-methylmercaptopurine metabolites in a single sample.* Journal of Chromatography B: Biomedical Sciences and Applications, 1992. **583**(1): p. 83-90.
25. Mawatari, H., et al., *Reversed-phase high-performance liquid chromatographic assay method for quantitating 6-mercaptopurine and its methylated and non-methylated*

metabolites in a single sample. Journal of Chromatography B: Biomedical Sciences and Applications, 1998. **716**(1): p. 392-396.

26. Wang, W., S.-F. Wang, and F. Xie, *An electrochemical sensor of non-electroactive drug 6-thioguanine based on the dsDNA/AET/Au.* Sensors and Actuators B: Chemical, 2006. **120**(1): p. 238-244.
27. Ensafi, A.A. and H. Karimi-Maleh, *Modified multiwall carbon nanotubes paste electrode as a sensor for simultaneous determination of 6-thioguanine and folic acid using ferrocenedicarboxylic acid as a mediator.* Journal of Electroanalytical Chemistry, 2010. **640**(1): p. 75-83.
28. Bi, N., et al., *Determination of 6-thioguanine based on localized surface plasmon resonance of gold nanoparticle.* Spectrochimica Acta Part A: Molecular and Biomolecular Spectroscopy, 2013. **107**: p. 24-30.
29. Kraske, P., *Electrochemical oxidation of 6-thioguanine.* Journal of electroanalytical chemistry and interfacial electrochemistry, 1986. **207**(1-2): p. 101-116.
30. Wang, Y., et al., *A FRET-based carbon dot–MnO2 nanosheet architecture for glutathione sensing in human whole blood samples.* Chemical Communications, 2015. **51**(64): p. 12748-12751.
31. Niu, L.-Y., et al., *BODIPY-based ratiometric fluorescent sensor for highly selective detection of glutathione over cysteine and homocysteine.* Journal of the American Chemical Society, 2012. **134**(46): p. 18928-18931.
32. Shen, X.-C., et al., *Determination of 6-mercaptopurine based on the fluorescence enhancement of Au nanoparticles.* Talanta, 2006. **69**(2): p. 456-462.
33. Wang, L. and Z. Zhang, *The study of oxidization fluorescence sensor with molecular imprinting polymer and its application for 6-mercaptopurine (6-MP) determination.* Talanta, 2008. **76**(4): p. 768-771.
34. Chen, Z., et al., *A fluorescence switch sensor for 6-mercaptopurine detection based on gold nanoparticles stabilized by biomacromolecule.* Biosensors and Bioelectronics, 2013. **41**: p. 844-847.
35. Du, J., Y. Wang, and W. Zhang, *Label- Free, Non- Derivatization CRET Detection Platform for 6- Mercaptopurine Based on the Distance- Dependent Optical Properties of Gold Nanoparticles.* Chemistry-A European Journal, 2012. **18**(27): p. 8540-8546.
36. Karimi-Maleh, H., et al., *A novel DNA biosensor based on a pencil graphite electrode modified with polypyrrole/functionalized multiwalled carbon nanotubes for*

determination of 6-mercaptopurine anticancer drug. Industrial & Engineering Chemistry Research, 2015. **54**(14): p. 3634-3639.

37. Li, H., et al., *Detection of 6-Thioguanine by surface-enhanced Raman scattering spectroscopy using silver nanoparticles-coated silicon wafer*. Colloids and Surfaces A: Physicochemical and Engineering Aspects, 2016. **493**: p. 52-58.
38. Amjadi, M., R. Shokri, and T. Hallaj, *Interaction of glucose‐derived carbon quantum dots with silver and gold nanoparticles and its application for the fluorescence detection of 6‐thioguanine.* Luminescence, 2017. **32**(3): p. 292-297.
39. Khalfaoui, M., et al., *New theoretical expressions for the five adsorption type isotherms classified by BET based on statistical physics treatment.* Journal of colloid and interface science, 2003. **263**(2): p. 350-356.
40. Du, J., Y. Wang, and W. Zhang, *Label‐Free, Non‐Derivatization CRET Detection Platform for 6‐Mercaptopurine Based on the Distance‐Dependent Optical Properties of Gold Nanoparticles.* Chemistry–A European Journal, 2012. **18**(27): p. 8540-8546.